Ph. D. Thesis

Development of hydrothermally stable catalysts for the valorization of ligno-cellulosic feedstocks to biofuels and renewable chemical platforms in hot liquid water

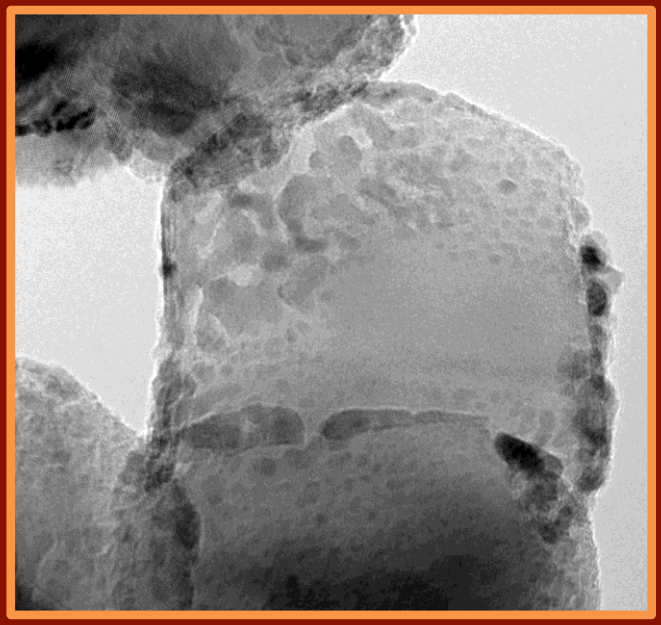

Nicolás Aranda Pérez

Dep. Chemical Engineering
Abengoa Research/ Escuela Técnica Superior de Ingeniería (Universidad de Sevilla)

2016

Tesis Doctoral
Ingeniería Química

Development of hydrothermally stable catalysts for the valorization of ligno-cellulosic feedstocks to biofuels and renewable chemical platforms in hot liquid water

Autor:

Nicolás Aranda Pérez

Director:

Jimmy A. Faria

Investigador Senior Abengoa Research

Dep. Ingeniería Química y Medioambiental

Escuela Técnica Superior de Ingeniería

Universidad de Sevilla

Sevilla, 2016

Tesis doctoral: Development of hydrothermally stable catalysts for the valorization of ligno-cellulosic feedstocks to biofuels and renewable chemical platforms in hot liquid water

Autor: Nicolás Aranda Pérez

Tutor: Pedro Ollero de Castro

El tribunal nombrado para juzgar el Proyecto arriba indicado, compuesto por los siguientes miembros:

Presidente:

Vocales:

Secretario:

Acuerdan otorgarle la calificación de:

Sevilla, 2016

El Secretario del Tribunal

A mi familia

"Experimentar es lo único que me motiva…es el acto en sí lo que me interesa, no el resultado, no me dejo impresionar por el mismo a no ser que la esencia me conduzca a ello"

Orson Welles

"The only real mistake is the one from which we can learn nothing"

Hernry Ford

Acknowledgements

Es de reconocer que este trabajo no hubiera sido realizable sin el apoyo y la ayuda de un gran número de profesionales con mayúsculas que aquí modestamente quería señalar.

En primer lugar, a la persona que me permitió la oportunidad de adentrarme en el estudio científico y director de la tesis doctoral Dr. Jimmy A. Faria con el que más cercanamente he trabajado y del que mucho he aprendido en estos años de investigación: sus continuas enseñanzas, criterio, aportaciones no sólo a nivel científico sino también personal han sido claves para el desarrollo de mi trayectoria tanto en la vertiente humana como técnica.

A continuación, a los investigadores senior del área a Dr. Juan Carlos Serrano y Dra. María Pilar Ruiz responsables en Abengoa del proyecto por sus siempre constructivas enseñazas y experiencia que enriquecían a los recién llegados con nuevas perspectivas y matices. Al Dr. Jesús Arauzo por sus indicaciones en aquellos comités de doctorandos donde compartíamos como grupo de investigación los avances en los distintos proyectos y que ponían bajo un mismo paraguas a investigadores senior y doctorandos favoreciendo el debate y

la aportación conjunta de ideas.

A los investigadores junior Dr. Javier Echave Lozano que estuvo encima en la primera etapa del doctorado en las actividades tanto de laboratorio como en la teoría su sólida formación y disposición a la enseñanza, su energía y capacidad de trabajo fueron para mí claves y por las que le estaré siempre agradecido. También me tengo que referir aquí al Dr. Manuel Antonio Díaz Perez por su siempre disposición mostrarme la importancia de no quere hacerlo todo a la vez, a su buen hacer, a su ayuda a lo largo de todo este período formativo en las más diversas situaciones y a la importancia dada en lo relativo a la seguridad y salud cuestión fundamental en un laboratorio.

Consecutivamente también me debo referir a D. Francisco Ladrón de Guevara con el que trabajé coordinadamente y del que aprendí su continua capacidad de resolver los problemas, integridad intelectual y ética y que ha sido también sin duda un referente en esta etapa. A Dña. Laura Sánchez por tantos ratos que compartimos también en el laboratorio, su profesionalidad y disponibilidad para ayudar siempre, gracias. A Dr. Juan Luis Sanz también por sus consejos y orientación.

Al conjunto de los investigadores juniors de las distintas áreas así como a los diversos técnicos de laboratorio también agradecer su capacidad para ayudar en todas las diversas necesidades que fueron surgiendo a lo largo de la investigación. Desde el Dr. Alejandro Herrero, Dra. Mercedes Lecea o el Dr. Gonzalo Rincón hasta Dr. Baldo Fernández o Eva y Almudena.

Por supuesto, no podría dejar de mencionar a los compañeros del doctorado juntos iniciamos una carrera en la que hemos vivido muchas dificultades y alegrías. Desde los más cercanos en el plano científico como Beatriz Gómez, Javier Moya, Irene Torija y Adrián hasta Javier Ramos, Irene Heras, Eva, Pau, Jacobo, Dani, Jonás, Toni, Lorena, María, Quique, Enrique, Sol, María, Zule,Emilio, Alejandro, Álvaro, Manu y Laura. A todos vosotros gracias.

También me quería referir a Dr. Santiago Medina de servicio de XRD y a su ayuda con la interpretación de los difractogramas y a Dr. Antonio Macías y Dra. Anna Penkova por su ayuda con el XPS del Centro de Investigación, Tecnología e Innovación de la Universidad de Sevilla.

No puedo terminar estas líneas sin referirme en esta etapa final del doctorado a dos personas: Dr. Pedro Ollero de Castro que ha sido el tutor que me ha orientado en relación a la Universidad y la Comisión de Doctorado así como permitirme continuar formándome en la misma y el Dr. José Antonio Odriozola por su sabiduría y conocimiento profundo científico. A ambos quedo en deuda.

Por último, quiero agradecer a mi familia por todo su apoyo y paciencia durante la realización de este trabajo.

Resumen

La realización de reacciones catalíticas en fase acuosa está adquiriendo un papel relevante debido a las ventajas que supone en términos de viabilidad económica, sinergias entre procesos catalíticos químicos y biológicos y por tratarse de un solvente no contaminante. Por tanto, desarrollo de materiales catalíticos hidrotérmicamente estables en agua es crucial para el desarrollo de estas reacciones anteriomente mencionadas en las que por un lado no se produzca el colapso de la estructura, ni lixiaviado del metal, así como desactivación del catalizador por competición en los sitios activos.

En esta tesis doctoral se ha realizado el diseño, la síntesis, la caracterización, prueba de actividad catalítica, cálculos cinéticos y de reciclabilidad de sólidos estables en fase acuosa para la reacción de cetonización de ácidos carboxílicos de cadena corta en cetonas. En concreto, se ha observado que, para el caso estudiado, la hidrofobización de materiales catalíticos sensibles al agua tiene como resultado la protección de éstos frente a su colapso o desactivación por la acción del agua en fase líquida permitiendo la reacción de las moléculas orgánicas, en esta trabajo se ha utilizado los ácidos carboxílicos presentes en la fase acuosa del bio-aceite (e. g. ácido acético). El estudio ha tratado tanto con moléculas modelo para la demostración de la prueba de concepto como con

fase acuosa de bio-aceite real donde las condiciones de trabajo son más arduas para el catalizador debido al alto número de compuestos presentes. Los estudios de reciclabilidad indican la actividad del catalizador persiste tras tres ensayos bajo condiciones de reacción.

Es también destacable que el escalado industrial de los catalizadores tanto en términos de acceso a los materiales, reproducibilidad y simplicidad de síntesis ha sido tenido en cuenta en el diseño de los mismos, y que los catalizadores diseñados podrían ser escalables, si bien serían necesarias pruebas adicionales en términos de estructuración de los mismos.

Esta metodología podría ser aplicada a otras reacciones de conversión de biomasa en fase líquida como son la hidrogenación de azúcares e incluso en procesos de reformado de alcoholes o procesos químicos donde la aparición de agua suponga un límite para la estabilidad y, por tanto para la actividad del catalizador.

Abstract

Performing catalytic reactions in aqueous phase is acquiring an important role because of the advantages in terms of economic viability, synergies between biological and chemical catalytic processes and for being a clean solvent. Therefore, development of hydrothermally stable catalytic materials in water is crucial to tackle the gap of knowledge present in before mentioned situations in which no collapse of the structure, nor metal leaching, neither catalyst deactivation by competition in active sites occurs.

This work has carried out the design, synthesis, characterization, catalytic activity tests, kinetic calculations and recyclability of stable solids in aqueous phase for the reaction of carboxylic acids ketonization short chain ketones. Specifically, it has been observed that, for the case studied, the hydrophobizing catalytic materials to water results in their protection against collapse or deactivation by the action of water in liquid phase enabling the reaction of organic molecules, in this work, particulary it has used the carboxylic acids present in the aqueous phase of the bio-oil (e.g. acetic acid). The study has performed tests on model molecules for demonstrating proof of concept as well as using real aqueous phase bio-oil where working conditions are more arduous for the catalyst due to the high number of compounds present.

Studies indicate recyclability catalyst activity persists after three trials under reaction conditions.

It is also noteworthy that the industrial scale of the catalysts both in terms of access to materials, reproducibility and ease of synthesis has been taken into account in the design, and catalysts manufactured could be scalable, although further evidence would be required in terms of structure.

This methodology could be applied to other conversion reactions of biomass in liquid phase such as the hydrogenation of sugars and even in reforming processes alcohols or chemical processes where the appearance of water represents a limit for the stability and thus for activity catalyst.

Index

TABLE OF FIGURES

List of abbreviations

μXRF	Microfluorescence of X-Rays
BET	Brunauer-Emmett-Teller
cos	Cosine function
CSTR	Continous Stirrer Tank Reactor
DFT	Density Functional Theory
FID	Flame Ionization Detector
HAADF-STEM	High Angle Annular Dark-Field Scanning Transmission Electron Microscopy
HRTEM	High-Resolution Transmission Electron Microscopy
TCD	Thermal Conductivity Detector
TEM	Transmission Electron Microscopy
TEM	Transmission Electron Microscopy
TGA	Thermogravimetric Analysis
THF	Tetrahydrofuran

XPS	X-Ray Photoelectron Spectroscopy
XRD	X-Ray Diffraction

1. GENERAL INTRODUCTION

This chapter will be devoted to the general description of the concepts required to understand the rest of the thesis. Additionally, the overall framework of the project in which this study is immersed will be also illustrated. These have been the two main targets which can be particularized as: i) the description of different routes of biomass derived feedstocks valorization by catalytic routes in liquid water; ii) the process of biofuels production from pyrolyisis oil, iii) the importance of stability in hot liquid water, and iv) the ketonization reaction as an intermediate route to stabilize bio-oil.

1.1. General Background

Biomass derived feedstocks (e.g. bio-oil) present generally a high degree of water content as has been widely posed in the literature (Gómez-Monedero, Bimbela, Arauzo, Faria, & Ruiz, 2015; Tessarolo et al., 2015; Wu, 2015). To reduce this aqueous presence normally energetically intense processes are required to evaporate this phase by torrefaction, heat exchangers or other costly separation processes that reduces this liquid element. However, an alternative approach has been to tackle this biomass derived feedstocks such as bio-ethanol or bio-oil with its water content and perform reactions in aqueous phase. This is a challenging step identified as critical in order to be able to couple bioprocesses with catalytic reactions as addressed by Dumesic et al. (Schwartz, Neill, Shanks, & Dumesic, 2014).

Among the different reactions interested to be performed in liquid phase, several of them have been identified as key and are reported in Figure 1-1.

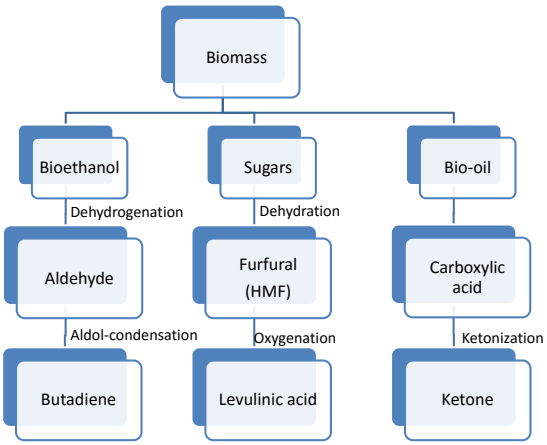

Figure 1-1.- Different reactions from biomass derived feedstocks to be performed in aqueous phase

In this thesis the focus has been devoted to ketonization reaction in liquid phase as the problem hydrothermal stability on aqueous environments is a major challenge for current state of the art catalysts. Furthermore, these materials investigated could be applied to other applications such as biomass conversion(Hernandez-Mejia et al., 2016), artificial photosynthesis(Yang, Yu, Linden, & Wu, 2010) or other industrial processes (Perez Ramirez, Mondelli, Schmidt, & Schluter, 2011).

1.2. Bio-oil upgrading processes

Bio-oil is produced by pyrolysis of non-edible lignocellulosic biomass from agricultural and forestry activities. Among the different thermochemical routes, this pyrolysis presents the advantage because of the conversion of large volumes of biomass into liquids(Mohan, Pittman, & Steele, 2006).

It is a complex mixture of organic acids, esters, furans, ketones, aldehydes and ethers, alcohols, phenolics, sugars and other compounds. The mixture keeps up to 70% of the energy stored in raw biomass, however, it presents a considerable number of oxygenated compounds, short C-C length and a high degree of water. The typical processing requires hydrotreating that consumes a significant amount of hydrogen which origin should be renewable to produce bio-fuels. Additionally, this treatment requires high pressures (up to 200 bar) and temperatures (between 300-400ºC) which overall makes it far from being market competitive with conventional non-renewable sources.

Alternatively to this costly process, CASCATBEL project (FP7 Grant Agreement nº 604307) proposed the design of a cascade procedure to couple condensation reactions, which do not require high pressures, temperatures or hydrogen consumption, with a final hydrodeoxygenation step to obtain advanced bio-fuels. The summary of this concept is described in Figure 1-2.

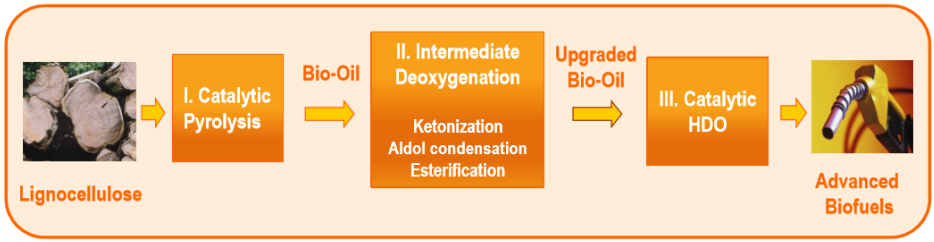

Figure 1-2.- Lignocellulose cascade deoxygenation ("CASCATBEL project," n.d.)

The three different routes explored in the project are: kenotization of short length carboxylic acids, aldol-condensation of aldehydes or ketones and esterification of organic acids and phenols. In all the three reactions the carbon length of the molecules is increased and deoxygenated targeting the formation of fuel like molecules.

This thesis has been focus on ketonization reaction in aqueous phase which poses different challenges: i) first, to reach the activations energies needed to the reaction to occur at low temperatures; ii) to avoid fast deactivation of the catalyst due to the effect of water molecules and iii) hydrothermal stability of the catalyst in aqueous phase to avoid collapse of the structure or leaching.

1.3. Ketonization reaction

Ketonization is a reaction starting from two short length carbolylic acids is able to convert them into ketone, carbon dioxide and water. The reaction particularized for the case of acetic acid is:

$$CH_3COOH + CH_3COOH \xrightarrow{catalyst} CH_3COCH_3 + CO_2 + H_2O \quad (1.1)$$

This reaction poses several features which are of paramount interest in case of bio-oil upgrading. Mainly, the increase in carbon length and decreasing the number of oxygens while decreasing significantly corrosiveness and; therefore, facilitates the storage of large amounts of bio-il. Additionally, it is relevant to point out that no need of hydrogen is required for this reaction to be performed.

The performance of this reaction in hot liquid water presents advantages from avoiding undesired polymerization side reactions and thermal decomposition of the pyrolysis oil as described by Resasco et al. (Tu Nguyet Pham, Shi, Sooknoi, & Resasco, 2012). Not to mention, that aqueous phase is the coherent medium to carry out the reaction since it is naturally present in the mixture.

Among the catalysts used in this reaction to occur transition metal oxides has been traditionally used in the past to carry out the reaction in vapor phase (Liu, Karim, Lebarbier, Mei, & Wang, 2013). In this study, high energy lattice metal oxides (e.g. TiO_2 and ZrO_2) have been utilized as a reducible oxide. Additionally, it has been impregnated with a metal (e. g. Ru and Ni) to enhance the reducibility of the support as will be described in chapter 3.

Regarding the reaction mechanism, there has been an excellent review from Resasco group(Tu N. Pham, Sooknoi, Crossley, & Resasco, 2013) in which different theoretical mechanisms are discussed. The most plausible route seems to be the deprotonation of the α-hydrogen, that creates the carbanion which attacks another organic acid molecule to form an intermediate β-ketoacid. Upon decomposition this molecule evolves towards the formation of ketones, water and carbon dioxide. Althought, there is still an open discussion on this materia.

DFT simulations have been carried out by Pacchioni to shed light on this issue. A recent paper from his research (Pacchioni, 2014) discusses the importance of Lewis acid and base sites in the surface of the catalyst, the role of pre-reduction of the metal deposited to favour the formation of Ti^{3+} sites and was further develop by his group (Ti, Tosoni, & Pacchioni, 2015). The latter supports the formation of these acid sites in some particular cases; however, a direct correlation of Ru clusters and increased reducibility of the support under hydrogen remains unclear. A final theoretical paper (Chen, Tosoni, & Pacchioni, 2015) indicates that hydrogen spillover effect, in which H_2 is dissociated into H atoms in the surface of the metal cluster and then diffuse to the surface of the metal oxide, has as a result, in case of a high coverage of hydrogen, the reduction of the support creating Ti^{3+} and Zr^{3+} centres on TiO_2 and ZrO_2 respectively.

Redox pairs seem to play a key role in the adsorption of the acid and favouring the deprotonation of the α-hydrogen. This hydrogen in the α position from the carbonyl group in the carboxylic acid is widely mentioned in the literature(Ignatchenko, 2011; Pestman, Koster, Duijne, Pieterse, & Ponec, 1997) as essential for the reaction to occur and to explain the mechanism beforementioned.

Therefore, acidity characterization studies of NH_3-TPD will be conducted to relate it with the activity of the catalyst as it seems to be an essential parameter to explain the catalyst performance.

Finally, it is important to comment on the research conducted on zeolites stabilization in hot liquid water(Zhang, Chen, Chen, & Resasco, 2015) has inspired the approach that led to innovative hydrothermally stable materials in aqueous phase. The dihydroxylation of the surfaces has as a consequence a increase in the hydrophobic behavior of the catalysts as indicated by (Kanta, Sedev, & Ralston, 2005); these concepts have led to the use of nearly hydrophobic materials stable in aqueous phase while maintaining its catalytic activity in hot liquid water.

2. EXPERIMENTAL TECHNIQUES FOR CHARACTERIZATION, CATALYTIC ACTIVITY AND ANALYTICAL METHODS

This chapter will be focus on the description of the experimental procedures and equipment used for catalyst characterization, measurement of catalytic activity and analytical methods.

The characterization techniques applied have been: i) determination of morphology and physical properties by N_2 isotherms, TEM (Transmission Electron Microscopy) and powder contact angle ii) surface properties by XPS (X-Ray Photoelectron Spectroscopy), iii) physico-chemical properties by XRD (X-Ray Diffraction), μXRF (X-Ray microfluorescence) and temperature programmed techniques.

Subsequently, catalytic tests are described in detail and both analyses will be correlated to identify causes of activity, limitations and improvements able to perform in order to overcome these burdens.

2.1. Characterization Techniques

In this section the different characterization of the catalysts will be described for the different materials synthesized.

2.1.1. X-Ray Diffraction (XRD)

It is an essential technique to identify crystalline phases, crystallographic parameters (e. g. unit cell dimensions, lattice symmetry or atomic coordinates) and physical/morphological features such as crystallite size, crystallinity, and preferred orientation of crystallites.

The equation that supports this technique is the Bragg´s Law:

$$n\lambda = 2d \sin\theta \qquad (2.1)$$

In this formula λ is the wavelength of the rays, θ is the angle between the incident rays, the surface of the crystal and d is the spacing between layers of atoms and n refers to a constructive interference when it is an integer.

Taking into account that the powders should be randomly oriented the X-rays are diffracted and detected so, by the Bragg´s low previously defined, it can be determined the lattice spacing on the material from the diffraction angle.

It is required that the material is enoughly crystalline (3-5 nm) to perform diffraction of the rays and they should in an amount greater than one percent.

The crystallite size of the metal loading has been calculated using the Scherrer equation:

$$B(2\theta) = \frac{K\lambda}{L\cos\theta} \qquad (2.2)$$

Where B is the peak width and it varies inversely with crystallite size L. K is the Scherrer constant, which only depends of how the width is determined, the shape of the crystallite and the size distribution. For this thesis K =0.94.

The equipment used was X-Ray Diffractometer D8 Advance A25 for powder (Bruker) with anode of Cu Kα radiation (40 kV, 30 mA) over a 2θ-range of 3 to 80 º. The detector used a step of 0.015º and a step time of 0.1s. The sensor used was sensitive to the position (Lynxeye).

Semi-cuantitative analysis of the phases was performed with software Diffrac.eva from Bruker.

2.1.2. X-Ray Microfluorescense (μXRF)

It is a non-destructive analysis that allows the identification and cuantification of elements at a trace level on the surface in solids or powder materials. It is ideal to identify components where XRD does not detect the elements.

This technique performs an elemental analysis for the examination of very small samples areas. The principle of operation is based in the direct X-ray interaction with different elements produce fluorescence identified by the sensor. In particular, micro X-Ray fluorescense (μXRF) uses an optic to resctrict the excitation beam therefore trace elements can be detected.

The equipment used was Eagle III of microfluorescense of X-rays (EDAX). It consists of a camera, which focuses the surface of the sample, and it can analyse the elements present qualitatively and quantitatively. The anod of the X-ray tube is made of rhodium working at 40kV, and the detector measure dispersive energies of this radiation.

2.1.3. X-Ray Photoelectron Spectroscopy (XPS)

This surface-sensitive quantitative spectroscopic technique is based on the determination of the binding energy of the electrons of the different elements present on the superficial layer of the sample (1.5 nm mean fee path).

In our case was used to determine the chemical or electronic state of Ru and Ti in the surface after a reduction treatment.

In this research, XPS analysis was carried out on a XPS-ESCA: PHOIBOS HSA3500 150 R6, the sample was previously reduced in a chamber in H_2 at 250 ºC for 1h, then transfer to the analysis chamber in ultrahigh vacuum conditions without exposure to air. A pass energy of 40 eV was used with an energy step of 1eV, analyser lens large area 1.5kV and in the scan mode fixed analyser transmission. Al $K\alpha_{1,2}$ radiation (1486.6 eV) was used as X-Ray source. The TiO_2 signals were adjusted to the C signal at 284.8 eV as an internal reference. The analysis of the data was conducted with CasaXPS software.

2.1.4. Textural properties: specific surface area, pore volume and pore size

The porous structure of the samples has been characterized using N_2 isotherms in which it can be quantified the volume adsorbed at different relative pressures at liquid nitrogen temperature (77K).

The value of the surface area was estimated by BET method. The pore size distribution was determined by the desorption derivative curve Barret-Joyner-Halenda (BJH) method. The micropore volume was calculated with t-plot method.

In this work, the experiments were conducted in a Micromeritics ASAP 2020 C. Before each analysis, the materials were degassed for 4h at 240 ºC in vacuum.

2.1.5. Transmission Electron Microscopy (TEM)

This technique was used to establish the morphology of the catalysts and the distribution of the metal loading over the surface of the catalysts. Additionally, TiO_2 crystal size was measured.

High angle annular dark-field scanning transmission electron microscopy (HAADF-STEM) and high-resolution transmission electron microscopy (HRTEM) characterization were carried out using a FEI Tecnai F30, operated at 300 kV equipped with a Gatan CCD camera, an EDS (EDAX) detector and a Gatam Tridiem Energy Filter. The sample was prepared by sonicating in N-butanol to improve the dispersion of the particles. The solution was dropped onto a holey carbon coated 300 mesh copper grid.

The calculus of the particle size of RuO_2 and TiO_2 was carried out with ImageJ software. Using more than 200 particles to estimate the average particle size and its standard deviation.

The particle dispersion was determined using the methodology defined by the US Patent (Larsson) US7,813, 523 B1 Oct. 12, 2010.

2.1.6. Thermogravimetric Analysis (TGA)

The TGA technique consists on measuring the weight change in the materialas a function of increasing temperature, isothermally in different atmospheres such as nitrogen or air. For this thesis, it was used to determine presence of organic compounds after the synthesis with a surfactant.

The equipment used was TGA-DSC Q 600 from TA Instruments. The sample was loaded, after drying at 100 ºC overnight, in the balance and heated under nitrogen flow (100 ml/min), heating ramp of 20 ºC/min up to 600 ºC.

2.1.7. Temperature Programmed Techniques

Different temperature programmed techniques have been used to establish several properties of the catalysts namely reduction temperature, acidity and carbon presence after synthesis.

2.1.7.1. Temperature Programmed Reduction

This technique is primarily used to determine the temperature at which the catalyst is reduced and to identify the time required to reduce completely the sample. It is fundamental in heterogeneous catalysis and it consists on passing through the sample a diluted mixture of H_2 on Argon, which has different response in the thermal conductivity detector (TCD), at a graduatelly increasing temperature.

In this work, TPR analysis of 100 mg of catalysts were conducted in Autochem 2920 using a gas mixture of 10%H_2 in Ar at a flow rate of 30 sccm with a linear heating ramp of 5 ºC/min up to 900 ºC and holding time of 1 min. H_2 consumption was determined by thermal conductivity detector.

2.1.7.2. Temperature Programmed Desorption of NH_3

This technique was used to determine the acidity of the catalyst, which played a critical role. It involved the cleaning of the surface with an inert gas, activation through reduction and finally a current of diluted ammonia on helium is pass through the sample at a constant temperature, then an inert gas is flowed again and finally a temperature ramp is conducted to determine at which temperature this ammonia is desorbed the higher the temperature the stronger acidity of the sample.

NH_3-TPD was carried out on Autochem 2920 using a gas mixture of 15% NH_3 in He. The surface was firstly clean with He, then it was reduced in 50 sscm of H_2 at 230 ºC during 3 h to replicate reduction conditions, then it was clean again with He at 230 ºC to evaporate any H_2O formed, once 35 ºC is reached, 15%NH_3/He is passed through the sample for 60 min in which it is chemisorbed, finally a temperature ramp of 10 ºC/min up to 900 ºC, to study the desorption profile, which is related to the acidity of the catalyst. In order to identify weak and moderate acid sites a temperature range of 50 ºC to 350 ºC (Barteau, Delmond; 1989) was selected and peak editor was used for integration.

2.1.8. Powder Contact Angle

The measurement of hydrophobicity of the catalyst has been performed based on Washburn equation in which the kinetics of adsorption of water is related to the powder contact angle. Surface tension and contact angle are related with the following equation:

$$\gamma_{sl} = \gamma_{sv} - \gamma_{lv} \cdot \cos\theta \qquad (2.3)$$

The definition of the reference of the powder contact angle is described in Figure 2-1.

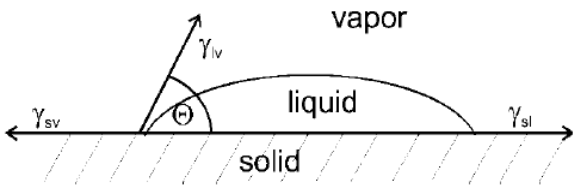

Figure 2-1.- Wetting of a solid with a liquid

DCAT 21 from Dataphysics was used for the weight-based measurement of the contact angle. First, a fixed amount of powder was compacted and tested in n-hexane to estimate the reference. Secondly, the same amount and degree of compactation was used to determine the powder contact angle.

2.2. Catalytic Activity

The reaction was carried out in a 150 mL batch reactor (Berghof BR-100) with a Teflon liner of 100 mL to avoid corrosion of the reactor. Firstly, 200 mg of catalyst was loaded on the liner, 65 mL of n-hexane (VWR, 99%) or deionized water depending on the experiment. In a first stage, the catalyst was reduced by placing the insert on the reactor and pressurized, after purged with N_2, with 30 bar of H2 stirring at 750 rpm, the reduction was conducted at 230°C and the pressure increased autogenously (60 bar) for 3h. After cooling the reactor to room temperature, the H_2 was purged and N_2 at 5 bar was introduced into the reactor. Then after a heating ramp of 2h, the target temperature of the reaction was reached (200°C, 210°C, 220°C depending on the experiment), at this moment, which indicates the starting time of the reaction, 7 mL of acetic acid are injected through an injection tank and the pressure was increased to 50 bar. Magnetic stirring was kept at 750 rpm to maintain the catalyst suspended to avoid mass transfer limitations. Reactions were run for 15', 30', 1h and 2h to establish the kinetics for each of the temperatures and time. Once the time of the reaction was completed, the reactor was quickly cool down to 10°C. Then, it was depressurized to ambient pressure and two liquid aliquots were taken for GC analysis and quantification. An Agilent Technologies 7890C GC equipped with an autosampler, autoinjector was used for quantification of the products and reactants. The column used for separating the constituents was HP-5 (30mx0.32 mm, 0.25μm).

In the case of real feeds, aqueous phase bio-oil, the introduction of the reactant was performed since the beginning of the heating ramp, to avoid possible contamination of the injection pipe. GC-MS analyses were carried out to

identify different compounds present on the aqueous phase and, after reaction, it was also analysed to identify products of reaction.

The recycling experiments were conducted following the same procedure aforementioned. After each reaction cycle the reactor effluent was filtered in a Nylon filter of 0.2 μm and dried overnight at 80°C. The dried catalyst was weighted and placed back inside the reactor for the next reaction experiment. To make the experiments comparable the catalyst to feed ratio was maintained constant (acetic acid:catalyst 1:0.61). The PID of the reactor was 200, 0.2 and 0 respectively.

Figure 2-2.-Reaction system: batch reactors, heating plates, injection tanks and control

2.3. Analytical methods

In this section the description of the techniques and equipment used for the analysis of reactant and products of reaction will be described.

2.3.1. Gas chromatography flame ionization detector (FID)

The quantification of the products and reactants was carried out in an Agilent 7890 B equipped with an FID detector. This apparatus used an HP-5 column of (30mx0.32 mm, 0.25μm) using helium as carrier gas.

It was used to quantify short-length carboxylic acids namely acetic acid, propionic acid and the corresponding ketones (e.g. acetone, propanone) as model compounds.

The operation conditions are described below:

- Carrier gas flow (He): 1.5mL/min
- Oven temperature: 40 ºC for 1 min; 2.5 ºC/min to 50 ºC for 0 min; 10 ºC min to 150 ºC/min for 1 min
- Detector temperature: 300 ºC
- H_2 flow: 40 mL/min
- Air flow: 450 mL/min

In case of bio-oil or aqueous phase bio-oil the method the mixture was far more complex and another method was implemented to analyse different families: carboxylic acids, aldehydes, ketones and ethers, furans, oxygenated aromatics and sugars.

The operation conditions are described below:

- Carrier gas flow (He): 1.2 mL/min
- Oven temperature: 30 ºC for 15 min; 15 ºC/min to 300 ºC for 10 min
- Detector temperature: 300 ºC
- H_2 flow: 40 mL/min
- Air flow: 450 mL/min

2.3.2. Gas chromatography with mass detector (GC-MS)

In order to identify molecular compounds present on bio-oil this characterization technique has been applied. The data base used for species assignment was NIST 14 mass spectral library. The operation conditions are defined in the following lines:

- Carrier gas flow (He): 1.2 mL/min
- Oven temperature: 30 ºC for 15 min; 15 ºC/min to 300 ºC for 10 min
- Detector temperature: 300 ºC
- H_2 flow: 40 mL/min

- Air flow: 450 mL/min

Ion source temperature 230 ºC, interface at 325 ºC, quadrupole temperature 150 ºC, electron ionization mode was set at 70 eV with a mass range of m/z 40-600 and the sampling rate was 1.36 $scans^{-1}$.

3. KETONIZATION REACTION OF ACETIC ACID. CATALYST SCREENING AND OPTIMIZATION

This chapter will describe the synthesis of an experimental matrix of catalysts of TiO_2 and ZrO_2 impregnated with Ru and Ni. Characterization techniques of these catalysts will be outlined. Afterwards, catalytic screening has been conducted to identify the best candidate for ketionization reaction in liquid phase. Further characterization of the best candidates will be commented.

3.1. Introduction

Ketonization reaction in liquid phase could play a critical role in bio-oil stabilization for further upgrading to advanced bio-fuels with a decrease on hydrogen consumption. Additionaly, the presence of high amount of oxygenated compounds and water make aqueous phase reaction an attractive proposition as energy intensive evaporation of bio-oil is avoided. From a chemical perspective, polymerization reactions are favoured at high temperature that could be prevented if the reaction is performed at low temperatures in liquid phase.

Regarding the catalysts selected, it has been identified that high energy lattice metal oxides (e.g. TiO_2, ZrO_2 and CeO_2) presents activity in vapour phase towards ketones from short length carboxylic acids (Tu N. Pham, Sooknoi, et al., 2013). The redox properties of the surface, allows the bi-dendate binding of the carboxylate (Ignatchenko, 2011) after deprotonation of the α-H of the organic acid, which is crucial for the nucleophilic carbanion formation. This attacks a nearby chemisorbed carbonyl-containing molecule to form an intermediate (e.g. β-ketoacid seems to be the more plausible), which is converted into a ketone, carbon dioxide, and water leaving the active site ready

for another catalytic cycle(Barteau, 1990; Xu, Iglesia, Apestegu, Cosimo, & Al, 1998)

The catalyst design approach has been to improve the reducibility of the metal oxide by impregnating Ru and Ni. A pre-reduction is conducted in order to increase the number of redox pairs and allow the catalyst to work at lower reaction temperatures. This hydrogen spillover effect on Ru clusters supported on TiO_2 and ZrO_2 has been studied by Pacchioni group (Chen et al., 2015) using Density Functional Theory (DFT) indicating the importance of high coverage of hydrogen on ruthenium in order to the spillover effect has on the support. In case of not presenting a high coverage the spillover will not take place.

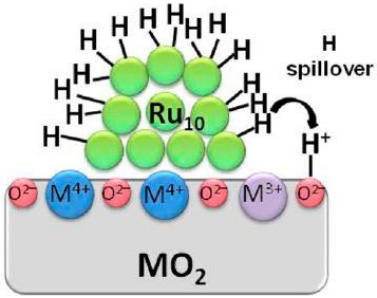

Figure 3-1.- Graphical description of H spillover effect from (Chen et al., 2015)

As can be observed in Figure 3-1 hydrogen is dissociated in metallic ruthenium and spill over the support in which reduction of the support takes place.

Among the different carboxylic acids present on bio-oil acetic acid has been selected as model compound for these catalytic tests. Detailed characterization

studies of different bio-oils reported by Aguado et.al indicated that acetic acid is in fact the most abundant organic acid, reaching concentrations as high as 10 %. Furthermore, stability studies have shown that this acid is the responsible for high corrosiveness of bio-oil (Aguado, Olazar, San José, Aguirre, & Bilbao, 2000).

Another aspect to analyse is the role of Ru in the catalytic mechanism of the reaction. Different studies indicate the action of Ru as agent that breaks C-CO bond producing a scission (Lu, Faheem, Behtash, & Heyden, 2015), although this effect by itself is not sufficient for the evolution into acetone; therefore, it is inferred the importance of redox sites of the support (e.g. TiO_2, ZrO_2) where the carboxylate is anchored in bidentate form after deprotonation of the α-hydrogen as discussed before.

3.2. Catalyst synthesis

The catalysts selected to be tested have been both commercial and lab synthesized of TiO_2, ZrO_2 and TiO_2-ZrO_2. Secondly, the impregnation with Ru and Ni on the supports has been performed using two different methods: incipient wetness impregnation and excess volume. In this section, the description of the different synthesis methods will be carried out. A summary of the different catalysts synthesized are shown in Table 3-1.

Table 3-1.- Catalyst matrix

Catalyst	Metal Loading (wt. %)	Synthesis method
5%Ru/TiO_2 P25	5	Excess volume
5%Ru/TiO_2 lab	5	Excess volume/ Sol-gel
5%Ru/ZrO_2 com	5	Excess volume
5%Ru/ZrO_2 lab	5	Excess volumen/Precip.
5%Ru/TiO_2 – ZrO_2	5	Excess volumen/Co-precip
5%Ni/TiO_2 P25	5	Excess volume
5%Ni/TiO_2 lab	5	Excess volume/ Sol-gel
5%Ni/ZrO_2 com	5	Excess volume
5%Ni/ZrO_2 lab	5	Excess volumen/Precip.

3.2.1. Support synthesis

Three main supports were lab manufactured to compare them with commercial ones. This will be denominated TiO_2 lab and ZrO_2 lab and TiO_2-ZrO_2 to distinguish them.

3.2.1.1. TiO_2 Synthesis

Sol-gel method was used as synthesis technique in case of titania. The precursor used was titanium isopropoxide (Sigma Aldrich, 99%). 20 grams of TiO_2 was manufactured in one batch to keep the same features of the catalyst for the different catalytic tests. Firstly, 74.14 mL of titanium (IV) isopropoxide were diluted in 222.43 mL of isopropanol. On the other hand, 3.7 L of deionized water were acidified to pH 2 by addition of HNO_3. Subsequently, the

formation of the gel came when both solutions were mixed and stirred vigorously. After the mixture became turbid, this was heated at 65 ºC for 20 h. Depending on the precipitation conditions; the resultant suspension was white-blue or opaque with high viscosity. The precipitate obtained was washed with ethanol (5 times) and was dried 100 ºC overnight. The resultant powder was white-yellow. Finally, this solid was calcined at 400 ºC for 2 h with a heating ramp of 2 ºC/min.

3.2.1.2. ZrO_2 Synthesis

Precipitation method was selected in case of zirconia. The first step consisted on dissolving 37.5 g of $Zr(NO_3)_2$ (Sigma Aldrich, 99%)up to a concentration of 0.4M. Secondly, ammonia (VWR, 30%) was slowly pour dropwise to allow the precipitation of the solid at a pH value of 10. After precipitation, the solid was aged at room temperature for 65h. Here, it was critical mantaining constant the pH during the ageing process. Then, the solid was washed 3 times with ethanol (VWR, 99%). Subsequently, the material was dried at 110 ºC for 12h. Finally, the support was calcined in air at 500 ºC for 10 hours with a heating ramp of 3 ºC/min.

3.2.1.3. TiO2-ZrO2 Synthesis

This mixed oxide was synthesized by sol-gel method. First, 800mL of deionized water was poured into a 1 L beaker and nitric acid added until the pH reached a value of 2. Separately, 8 mL of titanium isopropoxide (Sigma Aldrich, 99%) and 12 mL of zirconium propoxide (Sigma Aldrich, 99%) weredissolved on 45 mL of isopropanol (VWR, 99.98%). The content of this solution was gently spilled over the acid solution to initiate the hydrolysis. Afterwards, the solution was left 20 hours at 65 ºC. The resultant precipitate is

filtered; wash with ethanol and dried at 100 ºC overnight. Finally, it was grinded and calcined at 500 ºC for 6 hours to obtain a larger fraction of acid sites as studied by (Mao, Lu, & Chen, 2004).

3.2.2. Metal deposition

Ru and Ni were selected for the impregnation of the metal; due to different solubility coefficients of the precursor and activity under reaction conditions two impregnation methods were chosen: incipient wetness impregnation for nickel and excess volume impregnation for ruthenium.

TiO_2 P25 (Evonik), TiO_2 lab, ZrO_2 (Sigma Aldrich), ZrO_2 lab and TiO_2-ZrO_2 were all impreganted with a 5 wt. % metal loading .

3.2.2.1. Ru deposition

First, 0.513 g of $RuCl_3$ (99.98%, Sigma Aldrich) was dissolved in 0.5 L of deionized water for 5 g of support, and it was left under magnetic stirring (500 rpm) for 4 hours until complete dissolution of the salt was achieved. Afterwards, the corresponding amount of catalyst support was added to the solution and maintained under stirring overnight. In the following step, the dispersion was heated at 150 ºC and the water evaporated without boiling to allow the recrystallization of the solid. Subsequenltly, the solid was placed in the oven for 12 hours at 100 ºC. In the final step, the solid was grinded and sieved again and placed in the oven at 400 ºC for 4 hours to eliminate the chloride under air.

3.2.2.2. Ni deposition

In first place, measurement of pore volume of each support was conducted in order to determine the volume of water required to dissolve the precursor. Afterwards, $Ni(NO_3)_2$ $6H_2O$ (Sigma Aldrich, 99.99%) was dissolved in the calculated volume. The solution was added dropwise onto the support slowly, once the pores were filled, the solid was dried at 100 ºC. This procedure was repeated until the solution was finished. Finally, the material was dried at 100 ºC overnight and calcined at 400 ºC for 4 hours in air.

3.3. Results and discussion

Catalytic tests of the above mentioned materials were conducted in the experimental setup and reduction and reaction conditions described in section 2.2. Briefly, the 200 mg of catalyst were charged in the reactor in n-hexane (Sigma Aldrich, 99%), pressurized with H_2 at 30 bar and heated at 230 °C; once it returned to room temperature, the discontinuous reactor was depressurized and charged with N_2 and heated to 200 °C; at this time, the reactant (e.g. acetic acid) is injected which denotes the starting point of the reaction. The reaction takes place over time and it is stopped by rapid cooling in an ice tank. The comparison of the different catalytic activities of the solids in organic liquid phase is represented in Figure 3-3 and Figure 3-2

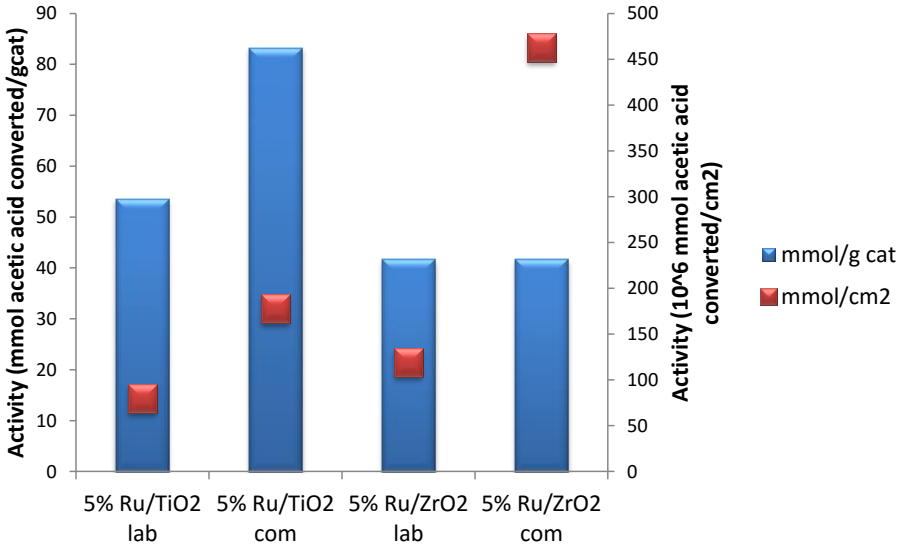

Figure 3-2.- Conversion of acetic acid over Ru impregnated catalysts.

From Figure 3-2 it can be noted that the highest catalytic activity was observed on Ru/TiO_2 com, even though its surface area (47 m^2/g) was lower than the laboratory synthesized Ru/TiO_2 (67 m^2/g). The reason for a greater conversion in the commercial TiO_2 could lie on the fact of the particular phases present in this support (20% rutile:80% anatase).

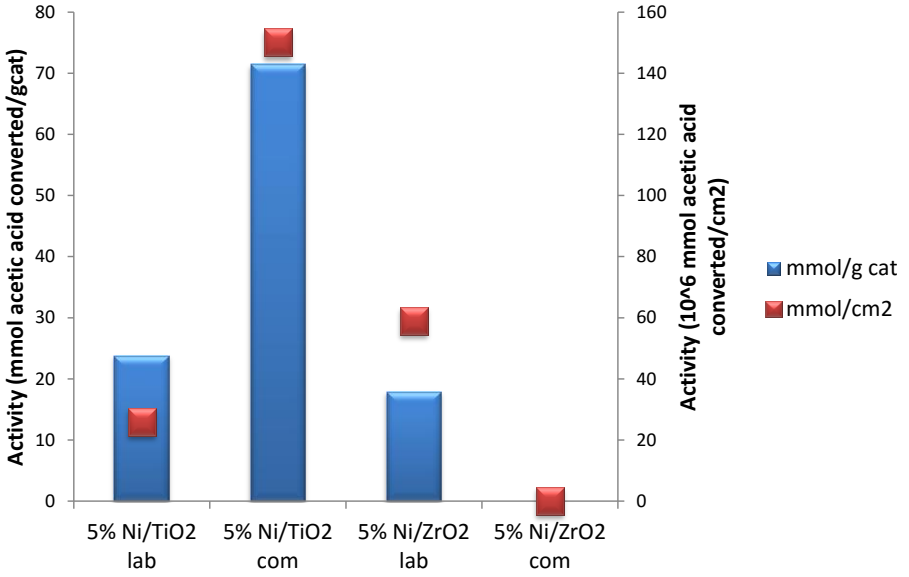

Figure 3-3.- Conversion of acetic acid over Ni impregnated catalysts.

Likewise to Ru based catalysts, solids with 5 wt. % Ni on TiO_2 and ZrO_2 have been prepared. In this case, as it can be seen in Figure 3-3, conversion values for these catalysts are considerably lower than those obtained on the same support impregnated with Ru.

This can be due to the fact that reduction temperatures of Ni based catalysts measured by TPR are around 400 ºC, which is not possible to reach in a previous reduction stage in liquid phase (system can only reach temperatures of 250 ºC). For this reason, these catalysts were reduced in a plug-flow reactor at 400 ºC, then passivated and, finally subjected to same reduction and reaction conditions than Ru based ones. However, even in that case, catalytic results were significantly lower than those of Ru impregnated catalysts.

The maximum conversion rate of Ni based catalysts was obtained when TiO_2 commercial (7%) was used as support, verifying the same trend observed for Ru based catalysts (see Figure 3-3). Comparing supports, Ni based catalysts follow again similar tendencies than Ru samples, Ni/TiO_2 com higher than lab synthesized one and, in case of Ni/ZrO_2 lab has a higher conversion than Ni/ZrO_2 com. This could be due to different reasons according to literature (Nagaoka, Takanabe, & Aika, 2004): first, noble metal decreases the reduction temperature and trigger hydrogen spillover that could generate a greater number of Ti^{3+} sites while Ni presents a significant higher reduction temperature which cannot be reached in the continuously stirred tank reactor (CSTR); second, Ni loading shows a higher degree of deactivation due to coke deposition.

From the results shown in figures above mentioned, it can be concluded that the performance of Ni based catalysts is significantly lower than for Ru based ones even though an additional stage of pre-reduction has been carried out. On the other hand, comparing supports titania shows higher conversion, independently of the metal loading, than zirconia in global terms. However, if we measure the activity per squared metre, which in case of ZrO_2 shows

considerably lower surface area, it presents higher activity.

In order to evaluate the effect of combining two amphoteric metal oxides with ruthenium catalysts the 5 wt. % Ru/TiO2-ZrO2 prepared by sol-gel was tested under reaction conditions. The conversion of acetic acid at the same reduction and reaction conditions was significantly lower than the one observed on 5% Ru/TiO_2 com reaching only 7% of acetic acid conversion. Thisdecrease in catalytic activity could be related to changes in the acidity of the material. As it is shown in Figure 3-4 NH_3-TPD profile indicates a significan shift of the desportion peak of NH_3 towards higher temperatures. Notably, on 5% Ru/TiO_2 com the main peak was centered at 300 °C, while in the case of 5%Ru/TiO_2-ZrO_2 a broaden peak centered at 450 °C wit a shoulder at 700 °C were observed. Clearly, utilizing ZrO_2 oxide with lower reducibility penalizes the formation of partially unsaturated metal cations, which in turns reduces the catalytic activity of the material(Benvenutti, Franken, & Moro, 1999).

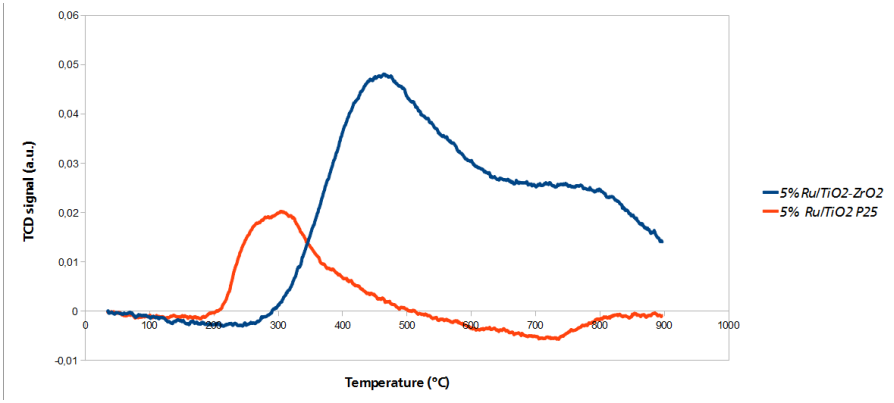

Figure 3-4.- NH_3 TPD profile of Ru/TiO_2 com and Ru/TiO_2-ZrO_2.

Different characterization techniques have been applied in order to understand the behavior of the most promising catalysts. In order characterize the porous structure of the different catalysts the surface area, pore volume and pore width has been measured by N_2 physisorption (see Table 3-1).

Tabla 3–1 Surface area, pore volumen and adsorption pore width of Ru and Ni impregnated catalysts.

Catalyst	S_{BET} (m^2/g)	Pore V (cm^3/g)	Pore D (nm)
TiO_2 lab	101	0.134	5
TiO_2 com	55	0.128	10
5%Ru/TiO_2 com	47	0.189	16
5%Ru/TiO_2 lab	67	0.128	8
5%Ni/TiO_2 com	48	0.184	15
5%Ni/TiO_2 lab	92	0.119	5
ZrO_2 lab	33	0.14	17
ZrO_2 com	5	0.014	11
5%Ru/ZrO_2 com	9	0.026	11
5%Ru/ZrO_2 lab	35	0.108	12
5%Ni/ZrO_2 com	5	0.016	12
5%Ni/ZrO_2 lab	31	0.09	12

From this textural data it can be induced that surface areas are substantially lower in case of ZrO_2 compared to TiO_2. Additionally, the impregnation with

the metal catalyst decreased the surface area of the material. Lab-synthesized samples presented higher specific surface areas, however, after impregnation and calcination these are considerably reduced. In terms of pore volume the most active catalyst (5%Ru/TiO_2 com) showed a pore volume of 16 nm, which is the highest of the series. Finally, in terms of pore size it is also among the highest (0.189 cm^3/g). The pore size distribution of TiO_2 based catalysts is described in Figure 3-5.- BJH Desorption DV/dlog(v) Pore Volume of TiO_2 based catalysts in which it is observed a more narrow distribution (4nm) in case of Ru/TiO2 lab while a wider porous distribution applied to commercial samples (between 20 to 50 nm). Metal deposition affects the porous diameter; Ni presents a displacement towards narrower pore diameters compared to Ru.

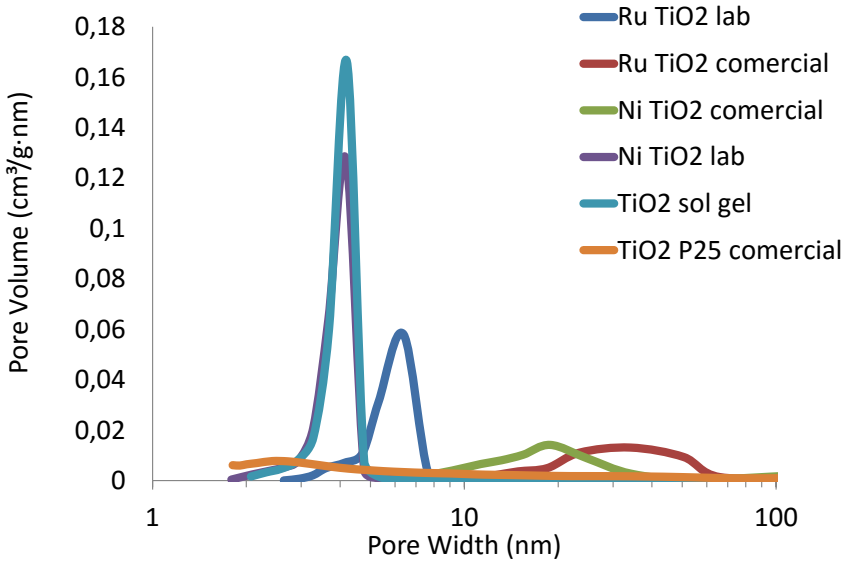

Figure 3-5.- BJH Desorption DV/dlog(v) Pore Volume of TiO_2 based catalysts

The crystalline structure of he most active catalysts and supports was characterized by XRD. The difractograms are shown in Figure 3-6.

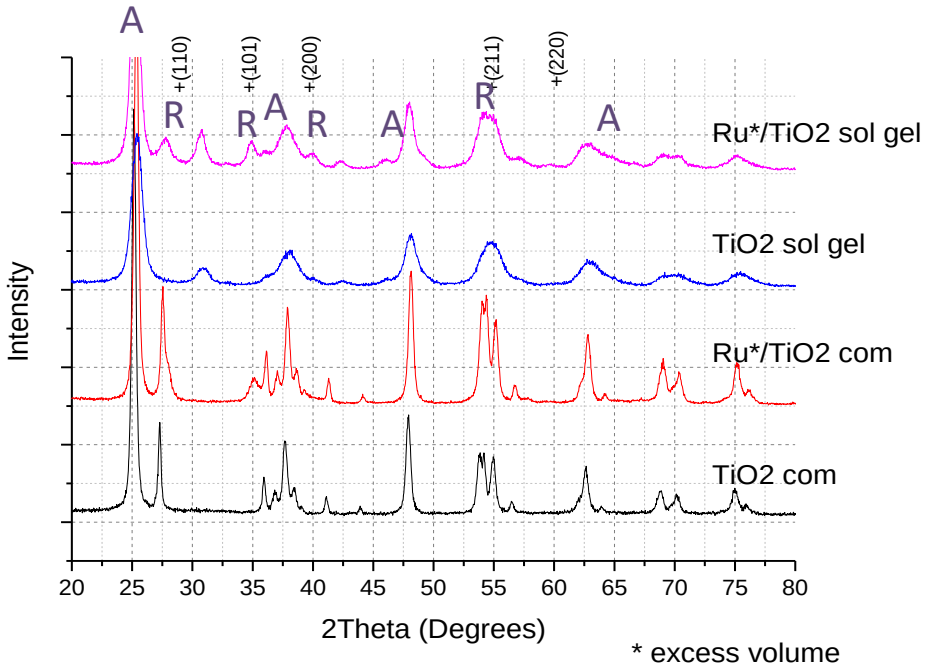

Figure 3-6.- XRD patterns of 5% Ru/ TiO_2 catalysts

(A refers to anatase and R to rutile)

This graph indicates that commercial samples presented anatase and rutile crystalline phases as expected from a TiO_2 P25, while in the case of lab synthesized TiO_2 anatase dominates. The planes observed in x, y, z: (110), (101), (200), (211) and (220) could be indexed to RuO2 rutile structure. Additionaly, commercial samples seems to show significantly higher

cristallynity than the ones synthesized due to the higher intensity of the diffraction peaks observed in the commercial catalysts compared to the lab prepared . The planes of RuO_2 present a rutile structure and therefore the diffraction peaks overlap with those of TiO_2 rutile. The amount of ruthenium deposited on TiO_2 was determined by X-Ray Microfluosrescense (Table 3-2). This semi-cuantitative technique was employed to determine the ratio of Ru to Ti or Zr for the different catalysts.

Table 3-2.- Ru loading, Ti and Zr content in the different catalysts.

Catalyst	Ti (wt%)	Zr (wt%)	Ru (wt%)	Ratio Ru:M
5%Ru/TiO_2 com	96.07	0	3.93	4
5%Ru/TiO_2 lab	92.95	0	6.13	6.6
5%Ru/ZrO_2 com	0	92.04	5.44	5.9
5%Ru/ZrO_2 lab	0	91.3	6.48	7
5%Ru/TiO_2-ZrO_2	39.02	54.54	4.32	11/8

Note: M denotes Zr or Ti depending on the catalyst sample.

The results indicated that depending on the deposition method employed the concentration of ruthenium can vary circa ± 1 %. Notably, in the case of TiO_2-ZrO_2 the mass ratio of Ti and Zr obtained (1:0.71) was slightly different from the expected value of 1:1 employed for the synthesis of the mixed oxide. The concentrations of Ti and Zr (obtained were 39% and 54%, respectively.. 5% Ru/TiO_2 com presented the lowest concentration of Ru among all the catalysts. Interestingly, this catalyst showed the highest activity (see Figure 3-2).

In the next chapter this contradictory result is discuss in detail.

Concerning the reducibility of the catalyst, TPR of the different materials have been performed to identify optimum reduction temperature and time of reduction. Complete reduction of RuO_2 will favour the effect of hydrogen spillover commented in section 3.1. As a consequence a higher number of partially unsaturated metal cations or Lewis acid sites will be generated in the surroundings of Ru particles. Furthermore, by comparing reduction temperatures of Ru and Ni it is possible to stablish reducibility and activity relationships that help to identify the most promising catalysts.

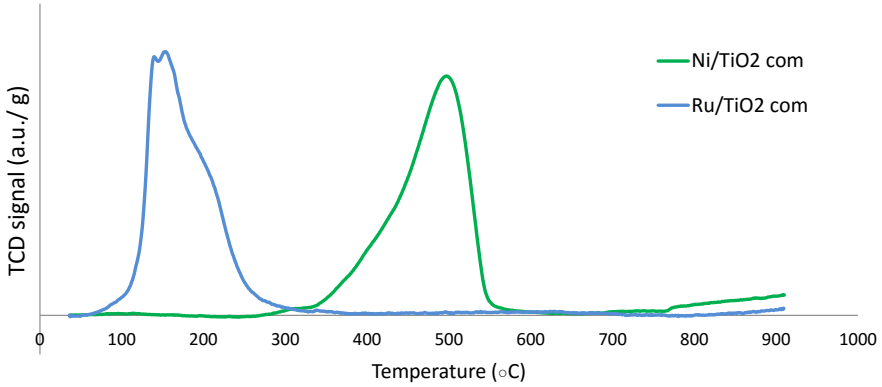

Figure 3-7.- Comparison of reduction temperatures of Ru and Ni.

From Figure 3-7 it is observed that reduction temperature of Ni (450 ºC) is considerably higher that the one obtained on Ru (200 ºC). Form the perspective of process operation the lower reduction temperature of Ru is highly desirable as it can be effectively reduced *in-situ*at mild conditions. Furthermore, the catalytic acitivity obtained on the Ru based catalysts is far

superior to the one observed on the Ni-based. The main drawback, however, is the cost of Ru. These catalysts employed 5 wt. % of ruthenium supported on TiO2; an exceedingly high loading. To improve the techno-economic feasibility of this process an optimization of the catalyst loading was performed. The results of this study are discussed in the following section When comparing the different catalysts(see Figure 2-1, Figure 3-8 and Figure 3-9), it can be observed that reduction of Ni and Ru occurs at slightly lower temperatures on zirconia compared to titania. Lab synthesized materials impregnated with ruthenium present a peak around 500 and 600 ºC that could be related to the solid solution of Ru in the crystal structure of the support. Different peaks shown in each of the TPR profiles Ru represent different species of ruthenium oxide.

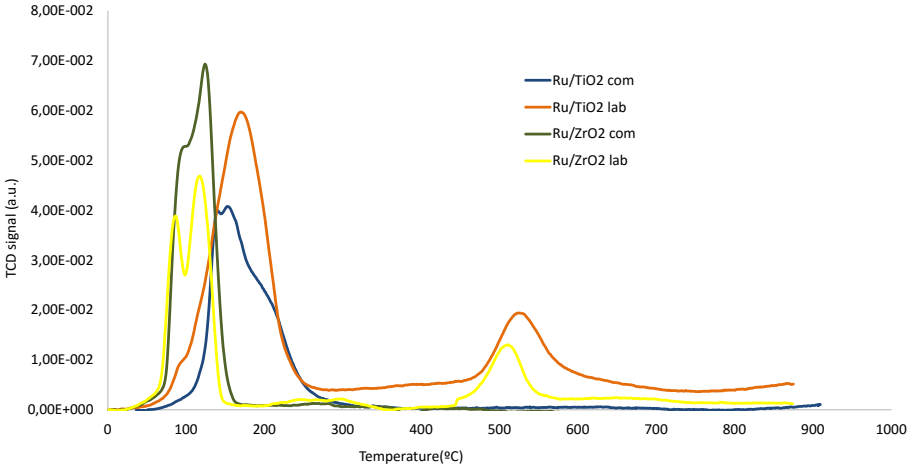

Figure 3-8.-TPR profiles of Ru based catalysts

As can be seen in Table 3-3.- Ru speciation based on H_2 consumption data, titania supports present mainly RuO_2 while over ZrO_2 other Ru species appear, and it seems that it depends on the support used.

Table 3-3.- Ru speciation based on H_2 consumption data

Catalyst	H_2 consumption measured	H_2 consumption calculated	Ru Species
5%Ru/TiO_2 com	106,74	98,15	RuO_2
5%Ru/ZrO_2 com	70,58	75,32	Ru_2O_3
5%Ru/TiO_2 lab	141,8	139,80	RuO_2
5% Ru/ZrO2 lab	60,5	63,8	Ru_2O_3

Regarding Ni based catalysts TPR, it can be observed a higher homogeneity in nickel oxide species in the profiles of commercial and lab synthesized titanias and on commercial zirconia as well.

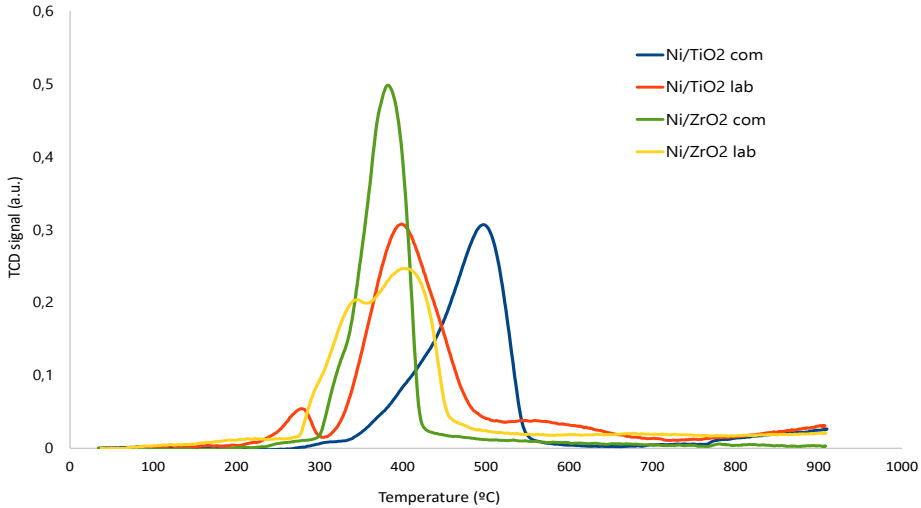

Figure 3-9.- TPR profile of Ni based catalysts

From calculation of hydrogen consumption versus measured as performed in case of ruthenium based catalysts, it is observed that the metal is reduced and the predominant oxide specie is NiO as is shown in Table 3-4. However, in this case, it seems that is not favouring the generation of oxygen vacancies in the surface of the support contrary of what occurs in Ru based catalysts.

Table 3-4.- Ni speciation based on H_2 consumption data

Catalyst	H_2 consumption measured	H_2 consumption calculated	Ni Species
5% Ni/ZrO_2 com	152,59	138,01	NiO
5% Ni/ZrO_2 lab	125,01	128,30	NiO
5% Ni/TiO_2 lab	120,88	139,80	NiO
5% Ni/TiO_2 com	137,63	143,29	NiO

Different characterization techniques applied indicate the importance of the support used, textural properties, reduction temperatures and the metal loading. In the next paragraphs different conditions of the reaction and changes in the catalyst have been analysed in order to be able to determine the optimum operation conditions and catalyst optimization.

First, it is important to highlight the effect of Ru loading, taking the most active catalyst different quantities of metal have been deposited in order to identify optimum Ru loading, which is of paramount significance since is the key cost of the whole manufacturing process. Two different metal loadings (1%, 0.5%) were deposited on TiO_2 P25 and tested under same reduction and reaction conditions. Results are displayed in Figure 3-10, as it is demonstrated a fivefold decrease on Ru loading has almost no effect in catalytic conversion of acetic acid into acetone.

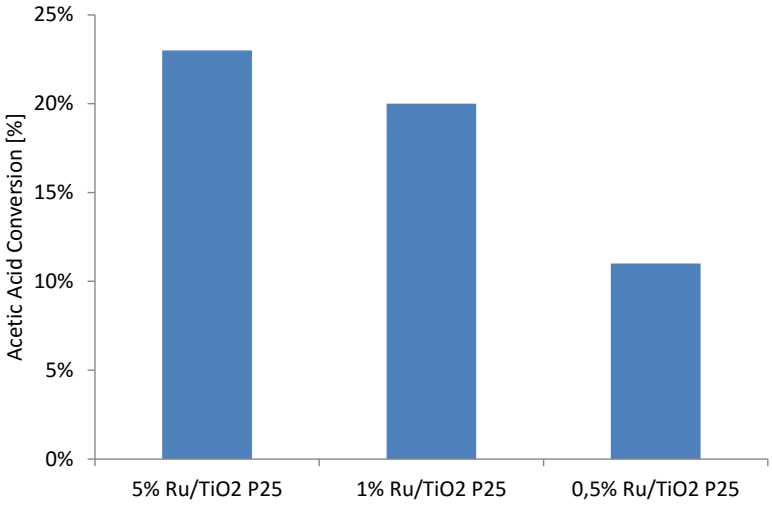

Figure 3-10.-Effect on conversion of different Ru loadings

Additionally the effect of higher length carboxylic acids (propionic acid) as model compound has been studied. In this case the most active catalyst has been tested in same reduction and reaction conditions but first catalytic tests in dicate that there is no conversion due to the higher carbon length and steric burdens of the molecule prevent the its conversion on Ru/TiO_2 com. As an alternative the use of other mixed oxides such as CeZrOx or CeMnOx have been other reducible oxides in which the conversion of propionic acid seems to be more favourable, although it is beyond the scope of this thesis.

Finally, the effect of reaction temperature on conversion has been evaluated. Three different temperatures were taken 180 ºC, 200 º ºC and 220 º ºC (Table 3-5).

Table 3-5.- Conversion results at different temperatures

Catalyst	X (180 ºC)	X(200 ºC)	X(220 ºC)
5% Ru/TiO_2 com	0%	23%	30%

The results show that no conversion at 180 ºC probably due to the not reaching the activation energy needed for the reaction to occur. While at 200 º ºC it increases due to a overcome of this energy barrier and at 220 ºC the conversion increases due to higher temperatures as expected by the Arrhenious equation.

3.4. Conclusions

Catalytic tests join to characterization studies have shown that the best catalyst is 5%Ru/TiO_2 com synthesized by excess volume method. It is important to highlight the effect of surface area, pore volume, presence of different phases, and moderate acidity of the catalyst, which favours the creation of oxygen vacancies. This titania P25 presents 80% anatase and 20% rutile. The next step in the investigation will be to conduct experiments in liquid phase in order to analyse the influence of TiO_2 phases on the catalytic conversion of acetic acid into ketones in liquid phase.

4. Effect of Titania Phases in Activity for Ketonization Reaction

5 % Ru/ TiO2 P25 has been proven as an effective catalyst for ketonization reaction under organic liquid phase. The purpose of this study is to investigate further the role of crystal phases of TiO_2 in ketonization reaction in liquid phase and highlight the effect of the phases in the hydrophobic or hydrophilic behavior in aqueous environments. This research would contribute to understand the effect of crystal phases in the increase of density of acid sites and in activation energies

4.1. Introduction

Bio-oil has a great amount of oxygenates and still has a low energy content to be a fuel. In addition, it presents a high reactivity and corrosiveness that makes it difficult to store as was pointed out by Ringer et al.(M. Ringer, 2006). Normally, several hydrogenation steps are required to reach a fuel-like energy content, but this upgrading has been proven to be uneconomical due to the great amount of H_2 consumed.

Several alternatives namely aldol-condesation, esterification and ketonization reactions have been proposed to decrease the oxygen content while increasing the carbon length and avoiding the use of hydrogen (Tu N. Pham, Shi, & Resasco, 2013a; Puértolas, Keller, Mitchell, & Pérez-Ramírez, 2016; Serrano-Ruiz & Dumesic, 2011; Zhu, Lobban, Mallinson, & Resasco, 2010). In this paper focus has been devoted to ketonization reaction in which carboxylic acids of short length (e. g. acetic acid) are converted into ketones, CO_2 and H_2O.

Following the research conducted by Resasco Group (Tu N. Pham, Shi, & Resasco, 2013b; Tu Nguyet Pham et al., 2012) that studied the use of high

energy lattice oxides such as 5%Ru/ TiO_2 for ketonization reaction in liquid phase; this study provides further insights in the role of this catalyst reaction in aqueous environments.

The model compound acetic acid has been selected as the most representative of short length carboxylic acids presents on bio-oil as described by Aguado et al. (Aguado et al., 2000).

Although different studies (Tu Nguyet Pham et al., 2012) have been focus on the catalytic activity of 5%Ru/TiO_2 for ketonization in liquid phase, the present contribution is aimed to analyse the role of titania phases (anatase, rutile and a mixture of both).

4.2. Catalyst synthesis

First, three different commercial TiO_2 were selected attending its phase composition: anatase (TiO_2 G5), rutile (TiO_2 Rutile), anatase/rutile in a proportion of 80/20 (TiO_2 P25). TiO_2 P25 and TiO_2 G5 were kindly provided by Evonik Industries and rutile was purchased to Sigma Aldrich. The three catalysts of the study were synthesized by excess volume impregnation. The Ru loading was 5 wt% using Ru (III) Chloride precursor (Sigma Aldrich, 99.98%). The required amount of the metal precursor was dissolved in deionized water and left for solution for 4 hours; subsequently TiO_2 was added and kept under stirring (500 rpm) overnight. Afterwards, evaporation of water was performed by heating at 150 ºC for 3 hours. Once the impregnation is accomplished, the catalyst was dried at 100 ºC overnight and finally calcined at 400 ºC for 4 hours with a heating ramp of 2 ºC/min. All samples followed the same preparation procedure. For this publication the catalysts will be labeled as TiO_2 anatase,

TiO_2 rutile and TiO_2 P25 (anatase/rutile).

4.3. Results and discussion

4.3.1. Catalyst characterization

Table 4-1 summarizes the BET surface area, pore volume and pore size of different catalysts and supports. The first point, to mention is than incorporation of Ru causes a decrease on the surface area of the catalyst in case of anatase and, interestingly in the case of rutile phase surface area is maintained. Secondly, the anatase phase present a higher surface area and pore volume of all the catalysts although during the calcination process at 400 ºC the structure of anatase is the most affected due to the presence of RuO_2.

Table 4-1.- BET surface area of the catalysts

Catalyst	BET Surface area (m^2/g)	Pore volume (cm^3/g)	Pore size (Å)
TiO_2 anatase	114.28	0.369	129
5% Ru/TiO_2 anatase	92.69	0.333	143
TiO_2 P25	54.63	0.128	94
5% Ru/TiO_2 P25	47.44	0.189	159
TiO_2 Rutile	23.36	0.144	247
5% Ru/TiO_2 Rutile	24.73	0.150	243

As shown in Figure 4-1, all materials are mesoporous and the adsorption-desorption hysteresis loop isotherm also change with phase composition. Additionally, BJH desorption curve has been used to determine the pore size distribution of the three catalysts (small graph). Rutile base catalyst presents a pore diameter significantly higher compare to those of anatase and P25 and, average pore size of anatase is nearer pore size of P25, which is 80% anatase/ 20% rutile.

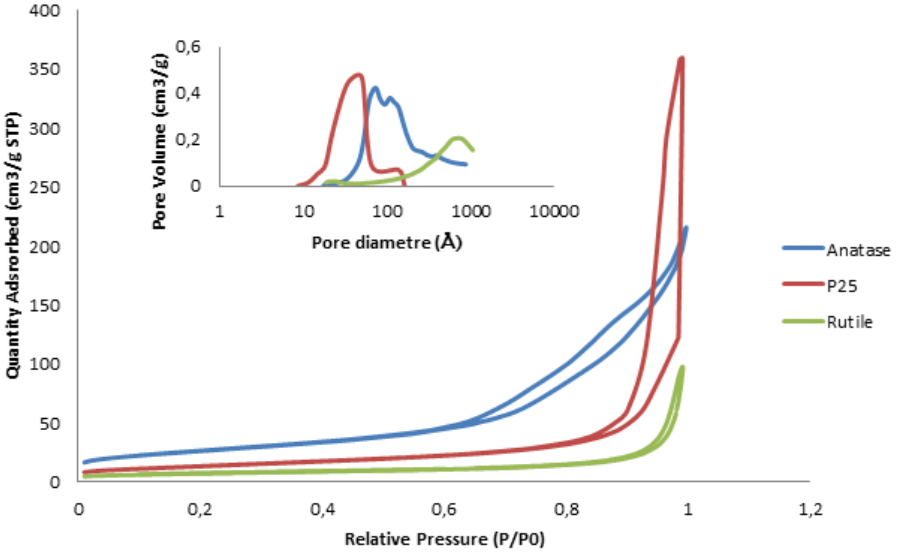

Figure 4-1.- N_2 isotherms and BJH desorption curve of anatase, rutile and P25

Concerning XPS characterization, it is observed no rests of Cl in the catalyst which indicates a correct calcination temperature and period. Additionally, in terms of Ru, two different ruthenium oxide species are observed before reduction and metallic Ru after the treatment at 250ºC under hydroghen atmosphere in 5% Ru/TiO_2 P25 and Rutile (Figure 4-2). In case of anatase due to impurities present on the sample data analysis was not appropriate to be performed.

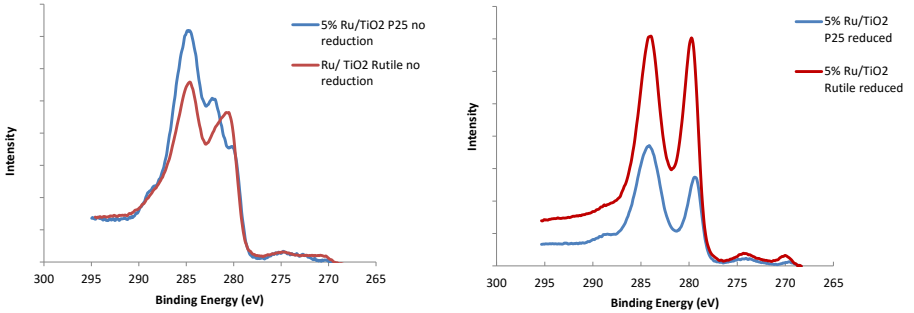

Figure 4-2.- XPS spectra of Ru/TiO2 rutile and P25 before and after reduction

In order to determine number of species RuOx present deconvolution of the curve has been carried out and it has been identified RuO_2 and Ru_2O_3 and metallic ruthenium (279,4 eV) after reduction.

Regarding TEM images (over 100 particles), displayed in Figure 4-3, it has been observed that the average size of Ru changes gradually depending on the phase present on TiO_2. Even though, anatase presents a higher surface area as shown before, more widely dispersed Ru nanoparticles are present in rutile as is described in Table 4-2.

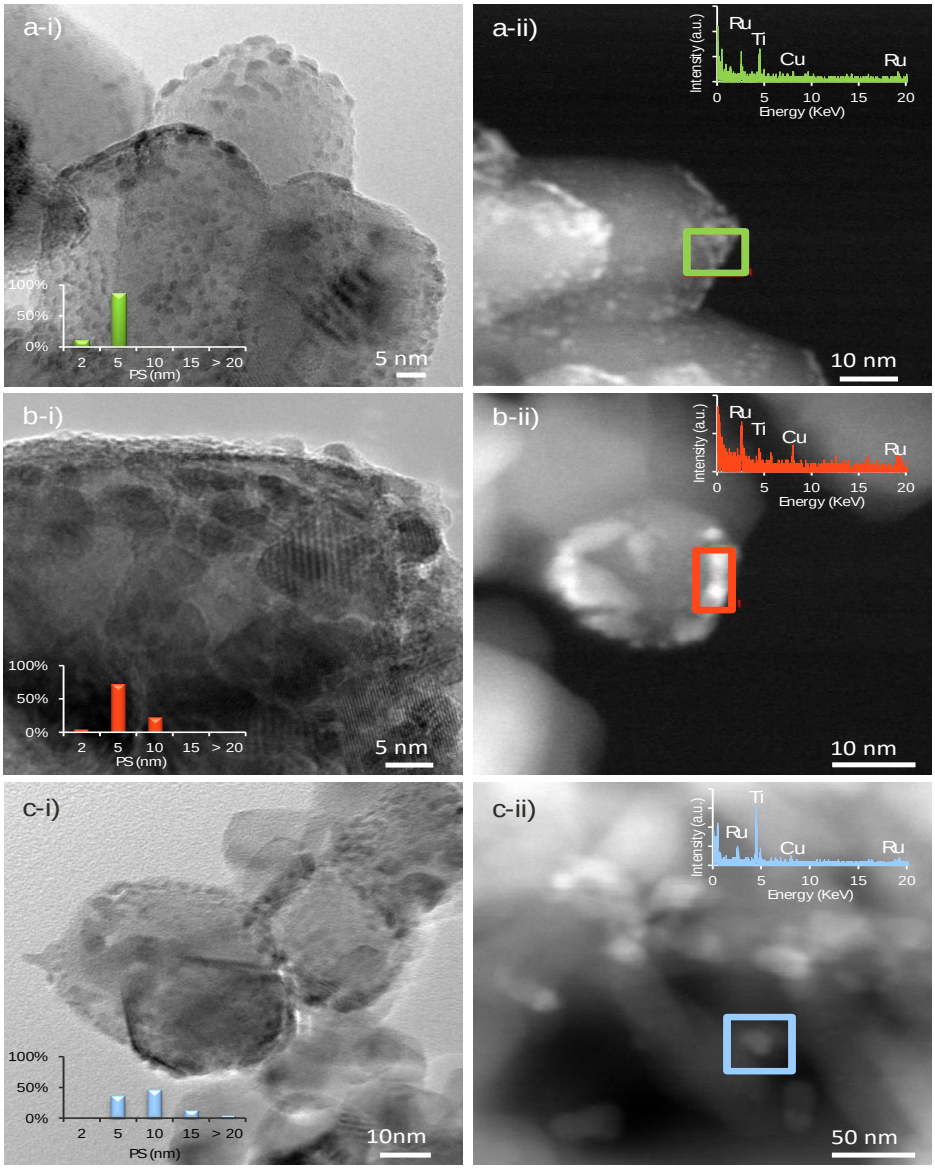

Figure 4-3.- TEM images of (a) 5% Ru/TiO2 Rutile

(b)5% Ru/TiO2 P25 (c) 5% Ru/TiO2 Anatase

As shown in Table 4-2, metal dispersion is higher in rutile phase due to the fact that RuO_2 and TiO_2 rutile present the same crystal structure (Hernandez-Mejia et al., 2016) a great loss in dispersion is observed on the anatase phase probably due to a decrease of the surface area during the calcination of the catalyst.

Table 4-2.- Particle size and metal dispersion of Ru calculated from TEM

Catalyst	Average size (nm)	Standard Deviation	Metal dispersión (%)
5% Ru/TiO_2 anatase	6.9	±3.66	12
5% Ru/TiO_2 P25	4.17	±1.61	24
5% Ru/TiO_2 Rutile	3.05	±3.05	31

Note: Metal dispersion has been estimated from TEM images following the method described in United States Patent (Larsson) US7,813,523 B1 Oct. 12, 2010

Ru particle size plays a crucial role on ketonization reaction in liquid phase since pre-reduction in H_2 favours a major improvement of the catalytic activity as was shown by Pham et al (Tu Nguyet Pham et al., 2012). This group performed EPR comparative analysis on TiO_2/C with and without Ru and they found the greater fraction of Ti^{3+} species that were formed with the noble

metal. In this work, we show that not only the Ru is critical but also the degree of dispersion of Ru in the support and the dependence on the crystal phase of TiO_2 and its effect for ketonization reaction.

XRD patterns of the catalysts (Figure 4-4) show a double fold target. First, the different phases of TiO_2 are clearly identified, indicating the anatase after calcination at 400 ºC is maintained, P25 is a mixture of a proportion of 80/20 anatase/rutile respectively. Rutile is the most stable phase and does not suffer any modification after impregnation with Ru and calcination. Second, RuO_2 matches the pattern in the JCPDS file, which indicates the formation of the oxide from the precursor in the synthesis stage. Peaks are observed in the graph but due to high dispersion, low loading percentage (5%) the signal is not strong enough to make a verification of the amount impregnated. Additionally, it is relevant to mention that in case of rutile there is an overlay on the peaks of RuO_2 and TiO_2 corroborating the results discuss before mentioned.

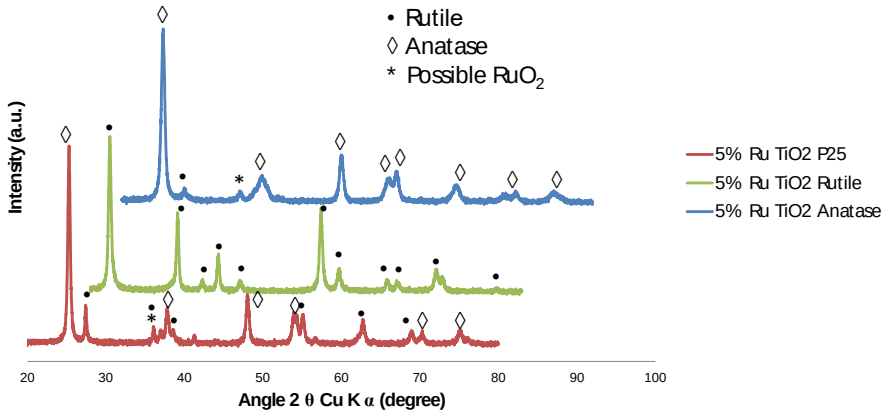

Figure 4-4.- Diffraction patterns of different catalysts anatase, rutile and P25

4.3.2. Catalytic performance of different phases TiO_2

Combined analysis of catalytic activity and dispersion (Figure 4-5.- Density of acid sites vs activity of the different TiO2 phases) confirm the increase of dispersion has as a result an improved conversion of acetic acid while in case of anatase and P25 (80% anatase) have similar conversion since the phases are practically the same. Even though there is a significant enhancement on dispersion in P25 in comparison to anatase the catalytic activity remains practically the same. Therefore, it is observed the important role of the phase in catalytic conversion of short-length carboxylic acids (e.g. acetic acid).

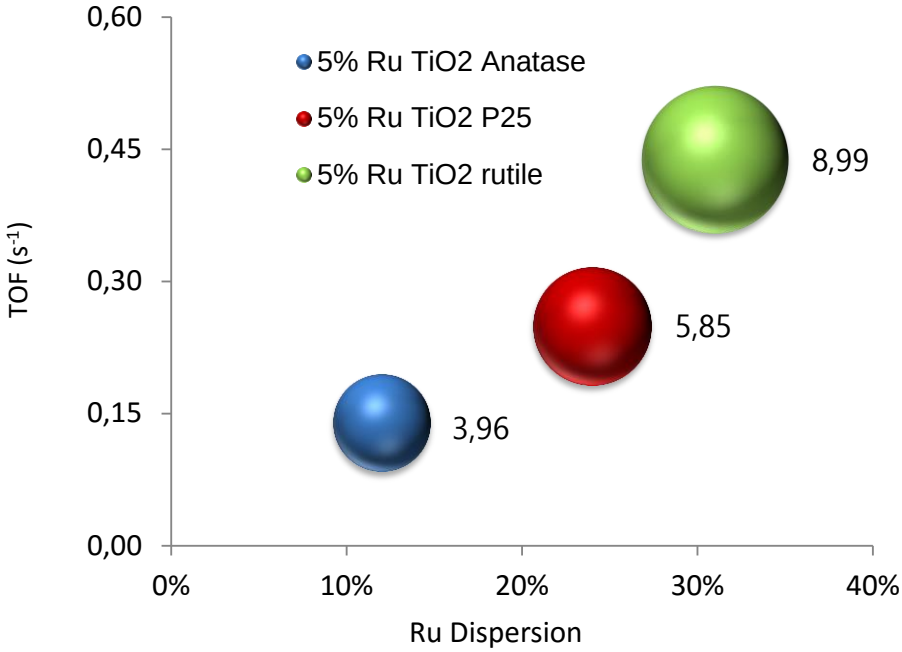

Figure 4-5.- Density of acid sites vs activity of the different TiO2 phases

This is also in agreement with characterization and catalytic activity measurements performed by Pham et al. (Tu Nguyet Pham et al., 2012), which pointed out the importance of prereduction in the enhancement of ketonization activity in aqueous phase.

Although deep investigations have been developed on the mechanism of reaction of ketonization reaction excellent reviewed by Pham et al. (Tu N. Pham, Shi, et al., 2013a; Tu N. Pham, Sooknoi, et al., 2013) and further discussed by DFT studies by Pacchioni and Pulido et al. (Pacchioni, 2014; Pulido, Oliver-Tomas, Renz, Boronat, & Corma, 2013) this is still a matter of debate. However, the most widely accepted mechanism seems to be the formation of a β-keto acid intermediate.

The conversion of acetic acid over the three catalysts has been evaluated at different times and temperatures in order to determine apparent activation energies for the different phases for ketonization reaction. The calculation has been done by calculating K at different temperatures of reaction and fitting experimental data by a power law model of order one. Arrherius plots of the different phases are shown in Figure 4-6.

First, its worthmention that mass transport limitations have been evaluated. Reaction order of n=1 with power law model have been used to fit the ketonization in liquid organic phase. Following the methodology of Vannice´s group (Mukherjee & Vannice, 2006), the Weitz-Prater criterion have been estimated. Taking into consideration that the value should be less than 0.3, it assures the lack of significant pore diffusion limitations.

$$\varphi_{W-P} = \frac{r_a \cdot R_P^{\,2}}{C_S \cdot D_{eff}} \tag{4.1}$$

Where r_a is the reaction rate per volume of catalyst, mol/m^3 s

R_P is the catalyst particle radius, m

C_S is the reactant concentration at the external surface of the catalyst, mol/m^3

D_{eff} is the effective diffusivity, m^2/s

The effective diffusivity has been calculated using Wilke-Chang estimation method (Wilke and Chang,1955).

$$D_{eff} = \frac{7.4x10^{-8} \cdot \left(\phi \cdot M_B\right)^{1/2} \cdot T}{\eta_B \cdot V_A^{\,0.6}} \tag{4.2}$$

Where D_{eff} is the diffusion coefficient, cm^2/s

ϕ is the association factor of solvent B, dimensionless

M_B is the molecular weight of solvent B, g/mol

T is the temperature, K

η_B is the viscosity of the solvent B, cP

V_A is the molar volume of solute A at isnormal boiling temperature, cm^2/mol

Particularizing this equation to our case of acetic acid on n-hexane, it is obtained a value of 4.95×10^{-5} cm^2/s. Once this value is known, a substitution in Weitz-Prater formula is performed (4.1). The resultant value is 0.0235, which fulfills the criteria and therefore absence of internal mass diffusion transport resistance is demonstrated.

The apparent activation energies are 187 kJ/mol in case of anatase and 89 kJ/mol for rutile. This is in accordance in the order of magnitude of those obtained in vapor phase ketonization for 5% Ru/TiO2 P25 (185 kJ/mol) as demonstrated by Pham et al (Tu N. Pham, Shi, et al., 2013b).

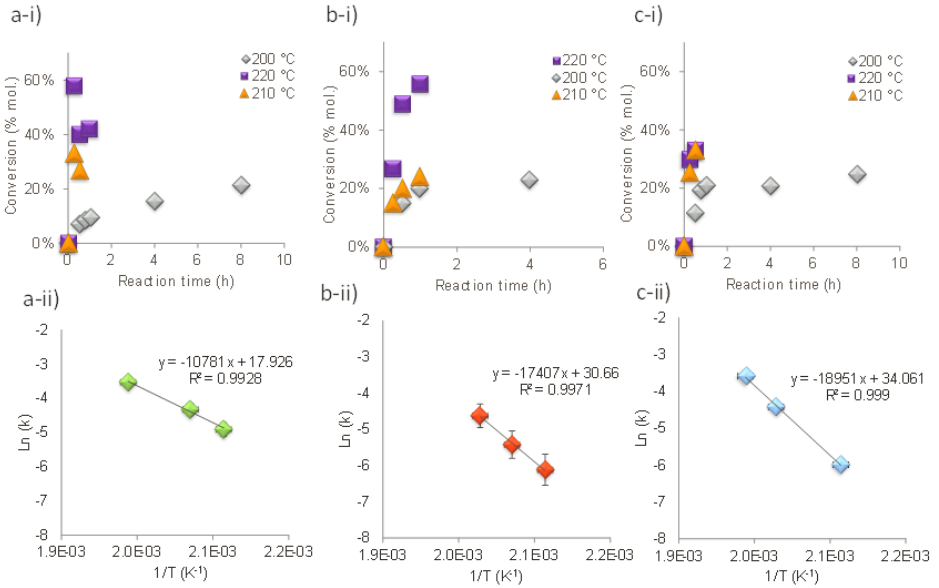

Figure 4-6.- Acetic acid conversion as function of time and Arrhenius plots for the decarboxylative coupling in liquid n-hexane at 200 °C (grey diamond), 210 °C (yellow triangle), and 220 °C (purple squares) on 5 wt. % Ru supported on TiO2 rutile (a i-ii), P25 (b i-ii), and anatase (c i-ii).

According to these graphs, it is also verified that the apparent activation energy on rutile phase is lower that on anatase phase. Therefore, it seems to support the previously mentioned statement that is not only a higher dispersion of the Ru on the surface what enhances ketonization but also the presence on the

rutile phase on titania. This effect could be explained by the differences in oxygen vacancies in the rutile compared to those in anatase. Simulation work carried out by Amore et al (Amore Bonapasta, Filippone, Mattioli, & Alippi, 2009) shed light on distinction in oxygen vacancies in different phases of TiO_2. They indicate the increase in concentration of oxygen vacancies under hydrogenation in rutile phase in comparison to anatase. Additionally, research conducted by Bouzoubaa et al (Bouzoubaa, Markovits, Calatayud, & Minot, 2005) support also a greater reducibility of the rutile phase versus anatase; therefore, forming a higher density of Ti^{3+} and having an positive effect in adsorption and reactivity on the surface due to this difference.

4.4. Conclusions

Crystal TiO_2 rutile phase plays a crucial role in ketonization reaction in liquid phase in two different aspects: (i) RuO_2 and TiO_2 Rutile present the same crystal structure, which has as a results higher dispersion of Ru particles, (ii) crystalline phase of rutile itself lower the activation energy for ketonization reaction. In the next chapter it will be studied correlation between this activity and its stability in hot liquid water.

5. HYDROPHOBIZATION OF TiO_2 FOR KETONIZATION IN HOT LIQUID WATER

Up to now, the study of the effect have been devoted to organic liquid phase; however, the goal of this thesis is to perform the reaction in aqueous phase and test the stability of the catalyst under these environments. For this reason powder contact angle measurements have been carried out in order to determine hydrophobicity of the different catalysts selected. Furthermore, catalytic activity over model compounds (e.g. acetic acid) will be evaluated under aqueous phase to establish the most hydrothermally stable catalyst for performing the reaction in these conditions of high water content which is the case of bio-oil.

5.1. Introduction

Biomass derived feedstocks such as bio-ethanol or bio-oil present a high degree of water content. This constitutes usually a drawback since energy intensive processes are required to evaporate this aqueous phase and obtain more energetically valuable products. The approach in this intermediate deoxygenation step has been to conduct it in presence of water avoiding this expensive evaporation process. Additionaly, it presents other advantages such as the avoidance of polymerization and oligomerization reactions since the reaction is carried out at mild temperatures (200-230ºC) and less energy consumption compared to vapour phase ketonization processes.

Other authors have tested different alternatives such as the hydrophobization by supporting the catalyst on active charcoal obtaining promising results(Tu Nguyet Pham et al., 2012). In our case, a doublefold perspective has been adopted: first, the study of the different phases in terms of its stability and

hydrophobicity in hot liquid water have been studied; second, alternative methods to hydrophobizise the surface of titania while maintaining its catalytic activity has been explored (e.g. the use of core-shell materials).

Up to our knowledge, this study of the powder contact angle of different titania phases and its effect in ketonization activity has no precedent in the literature.

5.2. Catalyst synthesis

Three catalysts of 5%Ru/TiO_2 Anatase, P25 and rutile were selected and synthesized as described in Chapter 4.

Additionally, TiO2-SiO2 core-shell materials kindly provided by Crystal (TiO_2 S545 and TiO_2 S1580) were calcined at 800ºC was conducted, in order to dehydroxylate the surface obtaining irreversibly siloxanes. The nomenclature of S545 and S1580 refers to the amount of silica present on the TiO_2 surface 5 and 10% respectively. Afterwards, an excess volume impregnation on methanol was carried out in a proportion of 100 mg of $RuCl_3$ (99%, Sigma Aldrich) for 100 ml of solvent. Firstly, the metal precursor was solved and, subsequently, the calcined core-shell support was introduced in the solution overnight. Once the mixture is homogeneus, the solvent was evaporated under mild stirring for 1h and dry in the oven for 12h. Finally, the catalyst is calcined at 400ºC for 4h with a temperature ramp of 2ºC/min.

For its interest, solvothermal method was applied to synthesize high surface area TiO_2 rutile. The method followed the instructions of Brinker´s publication (Jiang & Brinker, 2010). This method used Pebax 2533 kindly provided by

Arkema as directing agent to reach high surface areas after calcination maximixing porosity of the material, $TiCl_4$ (99%, Sigma Aldrich) and titanium isopropoxide (99%, Sigma Aldrich) to obtain the desired TiO_2 phase. Firstly, a solution of Pebax 2533 was solved in isopropanol (VWR, 99%) and stirred at 50ºC overnight obtaining a homogeneous mixture as described in Figure 5-1.- Solution of Pebax 2233 on isopropanol.

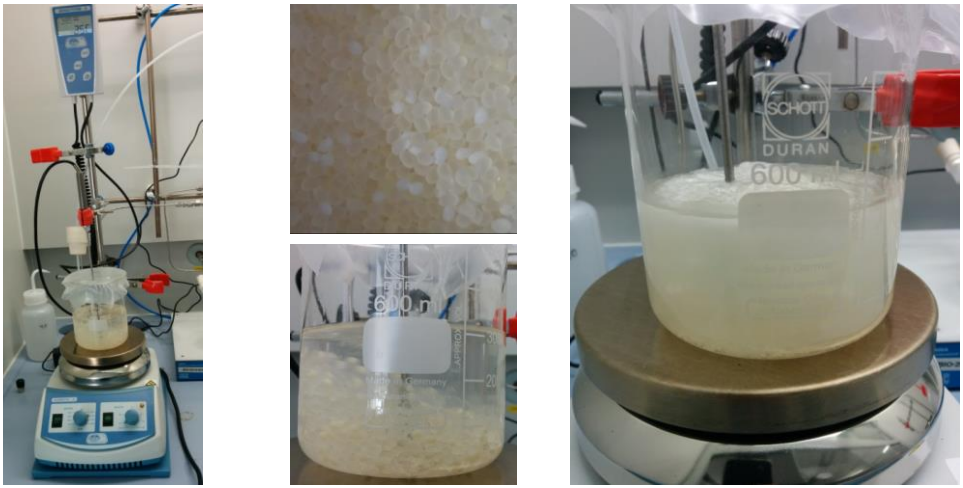

Figure 5-1.- Solution of Pebax 2233 on isopropanol

Then, titanium isopropoxide and chloride were added into the Pebax solution in an inert atmosphere at room temperature and stirring for 1 h. Subsequenltly, the temperature of the mixture was raised to 150ºC for 75 h in this inert environment (see Figure 5-2).

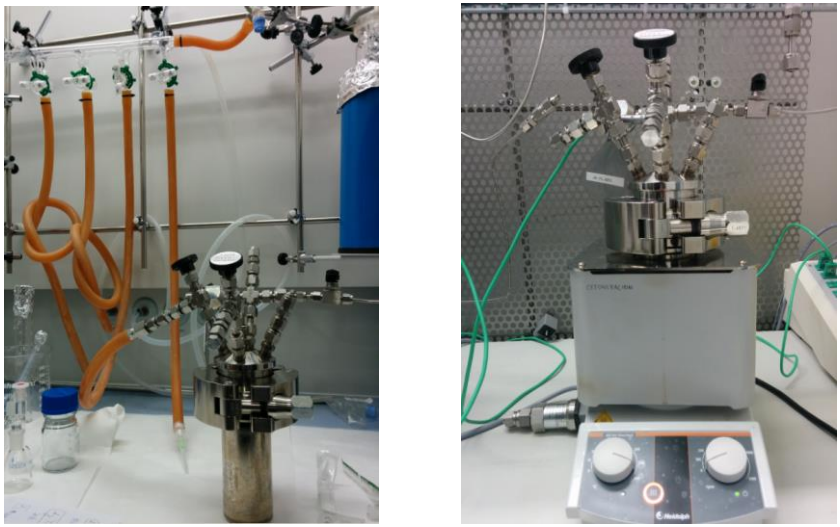

Figure 5-2.- Addition of the precursors in inert atmosphere and heating at 150ºC for 75h

A transparent titania/Pebax monolith is obtained. Finally, this solid is washed with isopropanol at 50ºC for 5-6 times to extract the polymer. A drying under vacuum conditions is performed to obtain a fine powder described in Figure 5-3

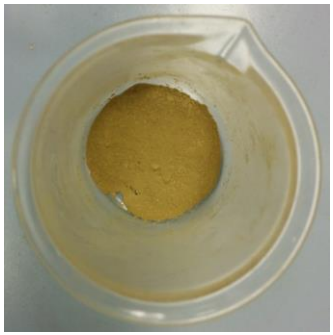

Figure 5-3.- Fine powder obtain after 5 times washing with isopropanol

5.3. Results and discussion

The powder contact angle of TiO_2 phases was measured in order to determine the hydrophobic hydrophilic balance of the samples, the results are shown in Figure 5-4. All the samples were calcined at 400 ºC for 4h before testing them at the tensiometer. As can be inmediatly observed, water adsorption curves of rutile are significantly lower that those of anatase and P25.

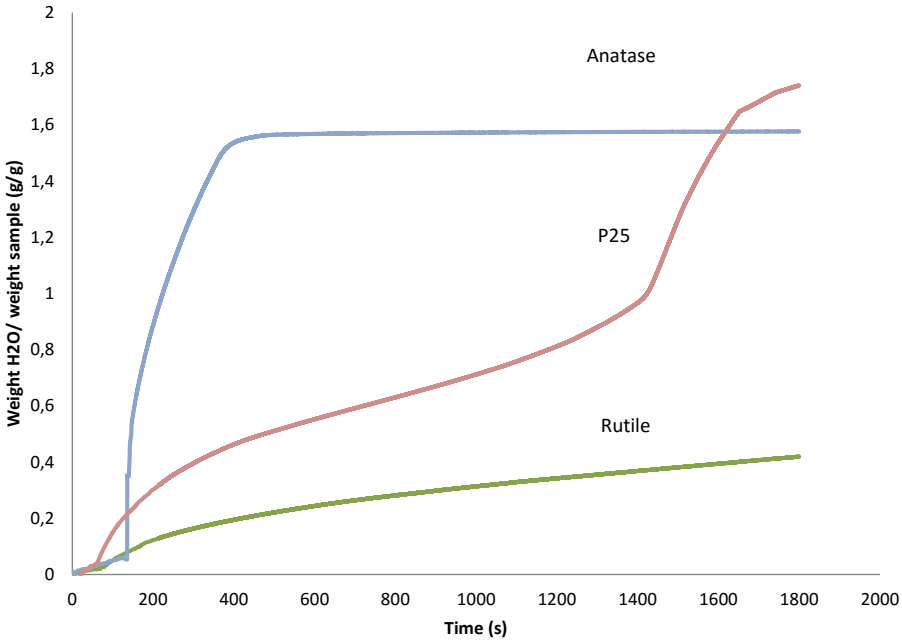

Figure 5-4.- Kinetics of water adsorption of different TiO_2 phases

Therefore, using these kinetics powder contact angle can be determined using Washburn equation as described in the publication of Teipel (Teipel & Mikonsaari, 2004). In Appendix B the description of calculation for contact angle of TiO2 P25 that presents two adsorption steps is performed. Summarizing, powder contact angles are shown in Figure 5-5.

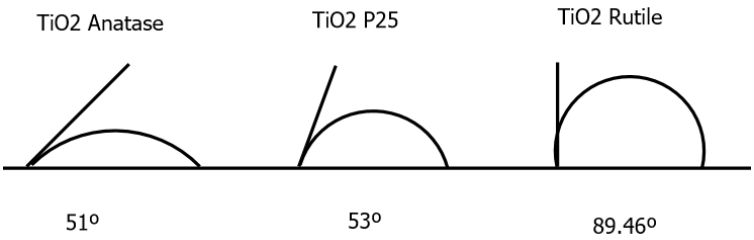

Figure 5-5.- Diagram of different contact angle of TiO_2 phases

This diagram shows the higher hydrophobicity of TiO_2 Rutile (89º) compared to P25 (53º) and anatase (51º) which major content is in anatase phase. This more hydrophobic behavior could be explained by the absence of surface defects terminated on –OH (Zhang et al., 2015). Additionally, catalytic tests were performed in aqueous phase to test the influence in activity of the different phases of TiO_2 and its hydrophobicity. Figure 5-6 shows that 5%Ru/TiO_2 Rutile present similar conversion of what is obtained in hexane while in case of anatase and P25 the deactivation is inmediate. There seems to be a direct correlation between hydrophobicity of the catalyst and its hydrothermal stability in water as indicates the following graph. In case of anatase and P25 where the powder contact angle is considerably lower than 90º it is quickly deactivated whereas for rutile (~90º) the stability makes it to maintain the activity of the catalyst across time.

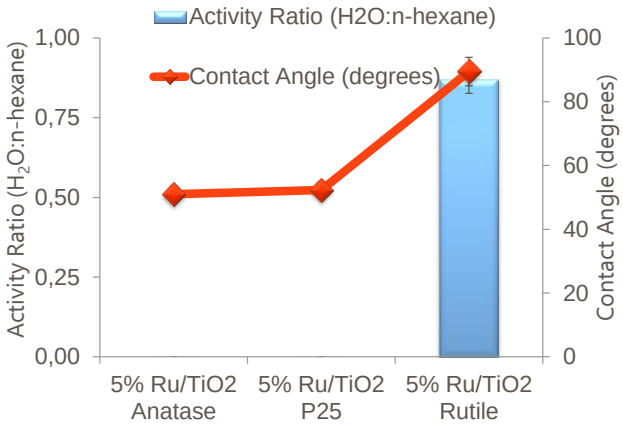

Figure 5-6.- Ratio of acetic acid conversion in liquid phase H_2O:n-hexane (blue bars a) over 5 wt. % Ru supported on TiO_2 anatase, P25, and rutile after 1 hour of reaction at 220 °C, 750 rpm, and 90 bar of N_2 in the presence of 200 mg of catalyst and 1.75 M of acetic acid dissolved in 35 ml of solvent. The catalyst was reduced in-situ at 230 °C, 750 rpm, and 30 bar of H_2 in 35 ml of solvent for 3 hours. Contact angle of the solid-H_2O-air interface of the different catalysts (red line a). Recyclability of the 5 wt. % Ru supported on TiO_2 rutile after several reactions at 200 °C

Reciclability tests were conducted to assess the ability of the catalyst to be active for different cycles. Notably, the catalytic activity and conversion remained almost unaltered for three different runs. Figure 5-7 shows this results in terms of catalytic activity; further studies could be carried out to determine if greater number of cycles could be reproduced by starting with higher catalyst mass and maintaining the catalyst to feed ratio.

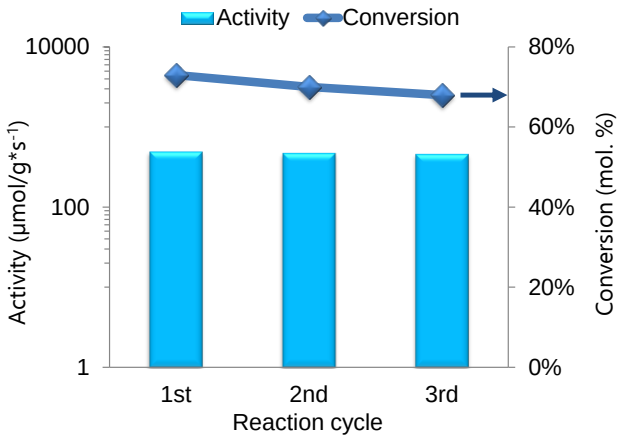

Figure 5-7.- Recyclability study of the 5 wt. % Ru supported on TiO_2 rutile after several reactions at 220 °C (b). Catalytic activity of the catalyst (µmol/g*s^{-1}) (light blue bars) and conversion of acetic (dark blue line).

Regarding the synthesis of high surface area rutile, it was characterized by XRD and results indicate that the forecasted rutile formation was not accomplished, even following the step by step method described in the paper.

The second strategy for the hydrothermal stability of TiO_2 catalysts was the utilization of TiO_2-SiO_2 core-shell materials, which calcined at 800ºC are dehydroxylated and; therefore, increased again the hydrophobicity of the material (Tosoni, Civalleri, & Ugliengo, 2010). The challenge was to keep the catalytic activity since the amount of SiO_2 could block TiO_2 pores and avoid conversion to acetone. The presence of SiO_2 had several advantages: on one hand, it maintained the surface area of TiO_2 even calcining at 800ºC because it retards the phase change of TiO_2, and; on the other hand, it was chemically inert for ketonization reaction and could be dehydroxylated and become more

hydrophobic for its stability under aqueous environments. Theoretically, the hypothesis was set; it remained to be proved that this could be achieved experimentally.

Two different 5%Ru/TiO_2-SiO_2 core-shell materials (see Figure 5-8) with different degrees of SiO_2 were prepared as detailed in section 5.2. In order to identify them in the next paragraphs, we will denote them as TiO_2-SiO_2 for the material with less silica content (5%) and TiO_2+SiO_2 for the solid with a higher SiO_2 amount (10%).

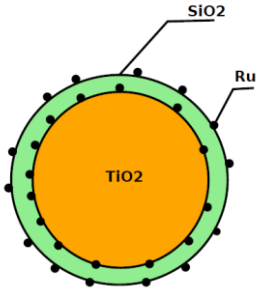

Figure 5-8.- Schematic representation of 5%Ru/TiO2-SiO2 catalyst

Different characterization techniques were applied to the material. Crystal structure of the catalyst was analysed to determine the presence of two phases in the material by XRD. Figure 5-9 indicates the different diffraction peaks of rutile and anatase and the amorphous region of SiO_2 seems to reveal the presence of two independent phases as was also observed by Watanabe group (Machida, Norimoto, & Watanabe, 1999). Interestingly, an increase on SiO_2 has a mitigation effect in the amount of rutile generated as was expected.

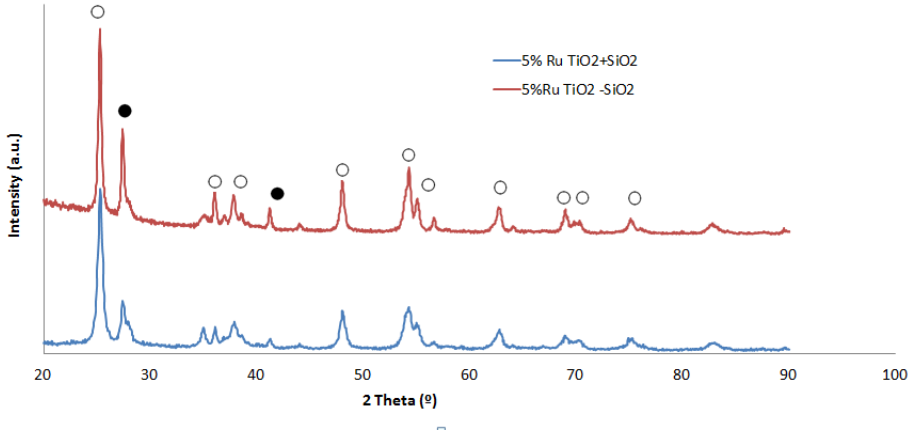

Figure 5-9.- XRD patterns of TiO2-SiO2 core-shell catalysts (● Rutile) and (○ anatase)

Additionally N_2 isotherms of the solid were evaluated to verify surface area resilience after calcination. Results displayed in Table 5-1 shows the stability in surface area even after calcination at 800ºC. It is important to note that pore of the less loaded TiO_2 presents a higher pore width which could be related to the access to the molecules to the active phase.

Table 5-1.- Textural parametres of core-shell catalysts

Catalyst	Surface Area (m^2/g)	Pore volume (cm^3/g)	Pore width (nm)
5% Ru/TiO_2 –SiO_2	49.92	0.46	37
5% Ru/TiO_2+SiO_2	64.39	0.32	19

Concerning catalytic activity measurements, the comparison test was carried out in an aqueous environment at the same conditions for reduction and reaction than previous experiments.

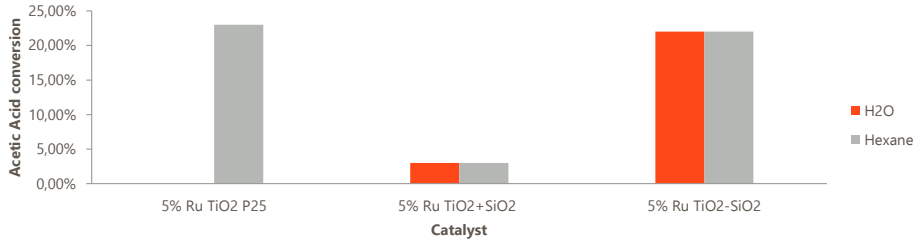

Figure 5-10.- Acetic acid conversion to acetone using as a solvent H2O (orange) and n-hexane (grey)

Figure 5-10 shows that core-shell material with a higher silica content present low conversion of acetic acid while the one with lower content present very similar activities that 5%Ru / TiO2 P25 the optimum candidate in organic phase. Additionaly, measuring powder contact angle in those materials conclusions were again supporting the importance of the amphiphilic behavior of the catalyst.

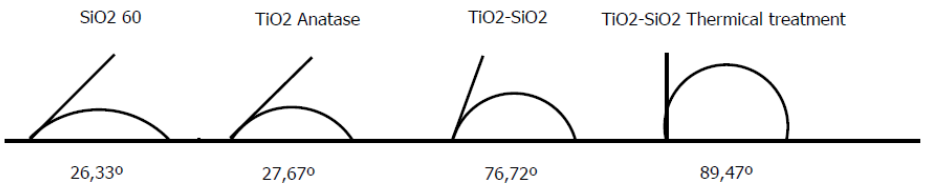

Figure 5-11.- Powder Contact Angle measurements of the different materials.

5.4. Conclusions

From this chapter it can be concluded that 5% Ru/TiO2 P25 is quickly deactivated in water environments. Alternatively, 5% Ru/TiO_2 Rutile presents hydrothermal stability in aqueous phase; therefore it is not only that the interface lattice matching effect of RuO_2 and TiO_2 Rutile boosts a higher dispersion of the metal on the catalyst but also its more hydrophobic behavior allows its stabilility in hot liquid water.

Additionally, TiO_2-SiO_2 core-shell materials shows stability in aqueous media and its low silica content allows the access to TiO_2 surface. Additionally, SiO_2 stabilizes surface area even calcining at high temperatures which are needed to dehydroxylate completely the surface increasing its hydrophobic behavior.

6. FROM MODEL COMPOUNDS TO REAL FEEDS. CATALYTIC TESTS WITH REAL BIOOIL

To finish up this thesis, the test with real aqueous phase bio-oil has been performed in order to demonstrate the ability of the catalysts to develop the reaction in real conditions. Given the promising performance with model compounds in hot liquid water, TiO_2-SiO_2 core-shell materials have been selected as catalysts to be proven under these unfavorable conditions. The aqueous phase bio-oil samples were kindly provided by IMDEA Energy. The procedure followed for its production was fast pyrolysis of woody biomass.

6.1. Introduction

In this chapter, aqueous phase bio-oil was characterized to identify its chemical composition and to see the evolution of reactants and products after reaction by GC-MS. Secondly, the reaction was conducted under similar conditions than in aforementioned chapters. Different solvents have been utilized to observe the effect of them in product distribution. Finally, some conclusions will be drawn from the enlightenment of the experimental results.

6.2. Catalyst synthesis

The materials selected in this section 5% Ru/ TiO_2-SiO_2 was exactly synthesized as those described in chapter 5. Briefly, TiO_2-SiO_2 was first calcined at 800ºC to trigger the irreversible formation of siloxanes with a hydrophobic character. Subsequently, this material was impregnated by excess volume impregnation. $RuCl_3$ (Sigma Aldrich, 99.9%) was solved in methanol instead of water in order to grant the deposition of the metal across the surface due to its hydrophobic behavior. Then, after 3 hours of stirring the support was added and left under same conditions overnight. Once the mixture was homogeneous, the solvent was evaporated and the resultant solid was dried at 100ºC overnight. Finally, the material was calcined at 400ºC for 4 hours with a ramp rate of 2ºC/min.

6.3. Results and discussion

Firstly, the characterization of aqueous phase bio-oil by GC-MS was conducted in order to identify the chemical composition of the samples and study the evolution of the compounds after reaction. The GC-MS method for the analysis is shown in chapter 2. The chromatogram with identification of the compounds distribution is shown in Figure 6-1.

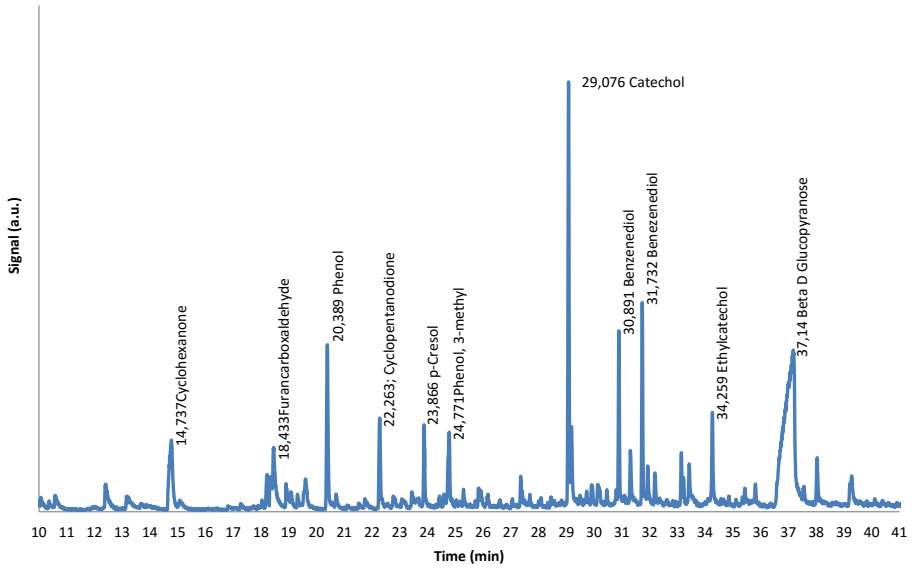

Figure 6-1.- Chromatogram of compounds distribution in aqueous phase bio-oil

As can be observed the typical chemical families of bio-oils appears in the graph: carboxylic acids, aldehydes, ketones and esthers, furans, aromatics and derived sugars. The proportion of these fractions present in aqueous phase bio-oil was analysed by IMDEA Energy and reproduced in Figure 6-2.

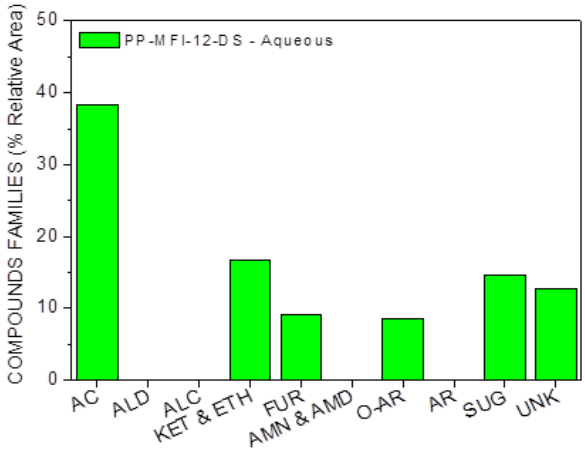

Figure 6-2.- Relative areas of chemical compounds in aqueous phase bio-oil (from IMDEA Energy analysis)

From this graph, it is observed the high amount of carboxylic acids present in this fraction of the bio-oil (37%), which is the highest among the different species present. In terms of concentration, the acetic acid was measured using a calibration curve in a GC-FID, results indicate 1,45M. First, the reaction was carried out in water as was planned at 220ºC for 1; after reduction of the catalyst at 230ºC for 3 hours. The outcome from the experiment is shown Figure 6-3. From the observation of the products, polymerization and oligomerization reactions take place forming a carbonaceous solid phase and an aqueous solution. Ideally, it is pursued to avoid the formation of two different phases; therefore, other solvents, namely n-hexane, methanol and THF, were tested to see its effect in the formation of a single liquid product.

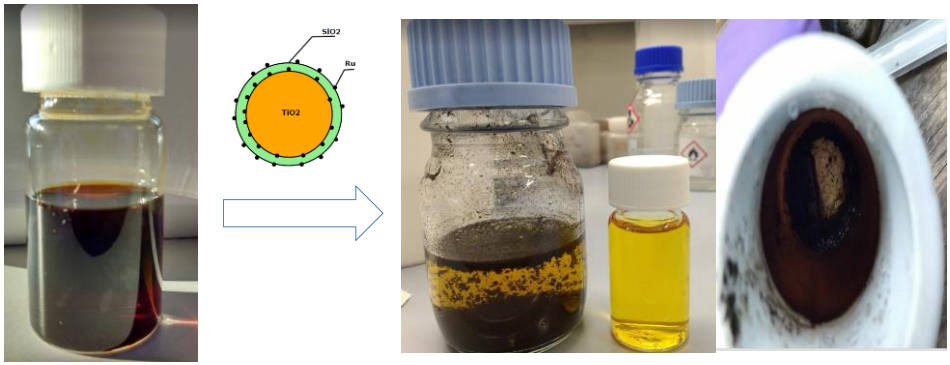

Figure 6-3.- Aqueous phase bio-oil and reaction products after reaction at 220ºC for 1hour in water environments.

The reaction with other solvents was conducted in the same conditions as those used in case of water, and products obtained are described in the following chromatograms by GC-MS.

First, the reaction with n-hexane formed a solid and two liquid phases due to is organic character only solved organic compounds. Additionally, identification of products shows the formation of hydroxymethylfurfural (HMF) as detailed in Figure 6-4.

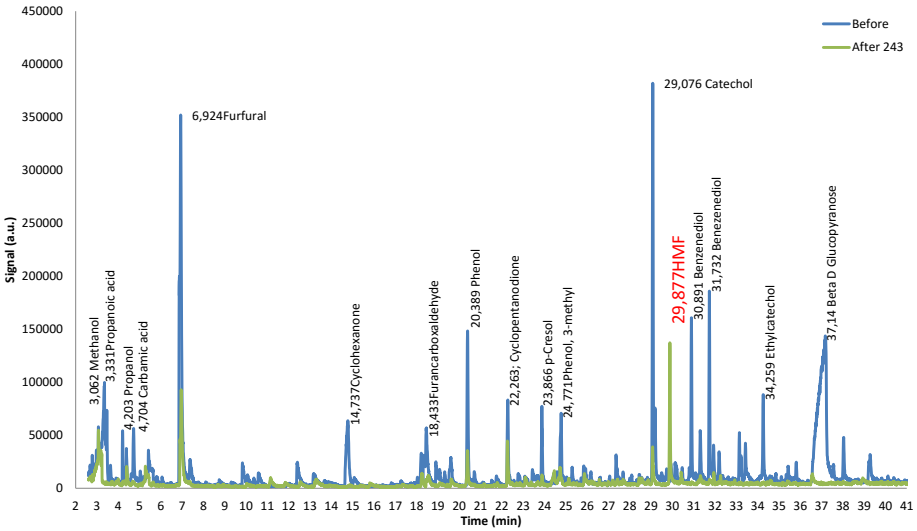

Figure 6-4.- Chromatogram before and after reaction using as a solvent n-hexane.

In case of methanol, only one phase was observed due to the ability of the solvent to solve polar and non-polar molecules. However, esterification and aldol condensations reactions take place due to the presence of the methanol forming glycoaldehyde as demonstrated from Figure 6-5.

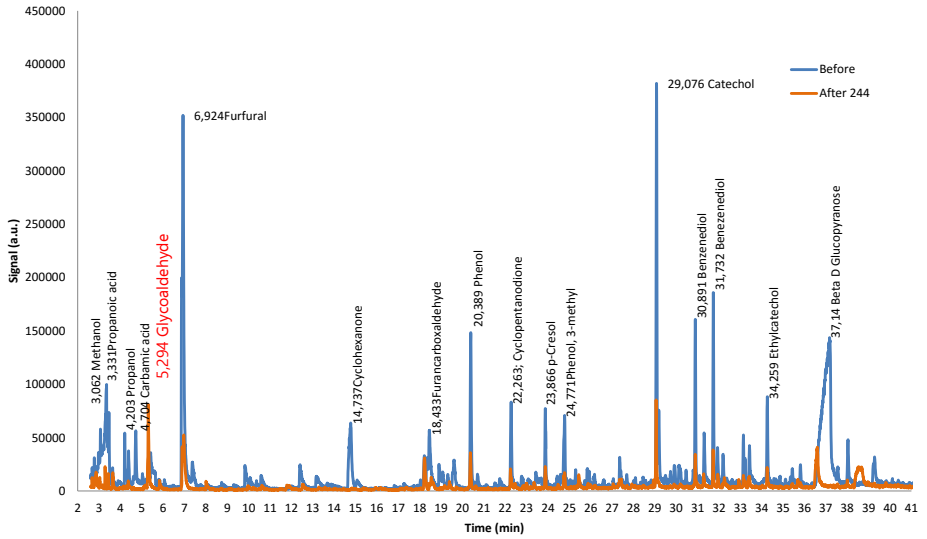

Figure 6-5.- Chromatogram before and after reaction using as a solvent methanol.

Therefore a last solvent was tested with the same properties of methanol of solving aqueous and organic phases to reach a single phase product and without interaction with the reactants. The solvent that fulfills this criterion was THF. Results from Figure 6-6 shows that there is no interaction with the solvent but no other products are formed and it present a major drawback of not being a green solvent and its non probable scalability.

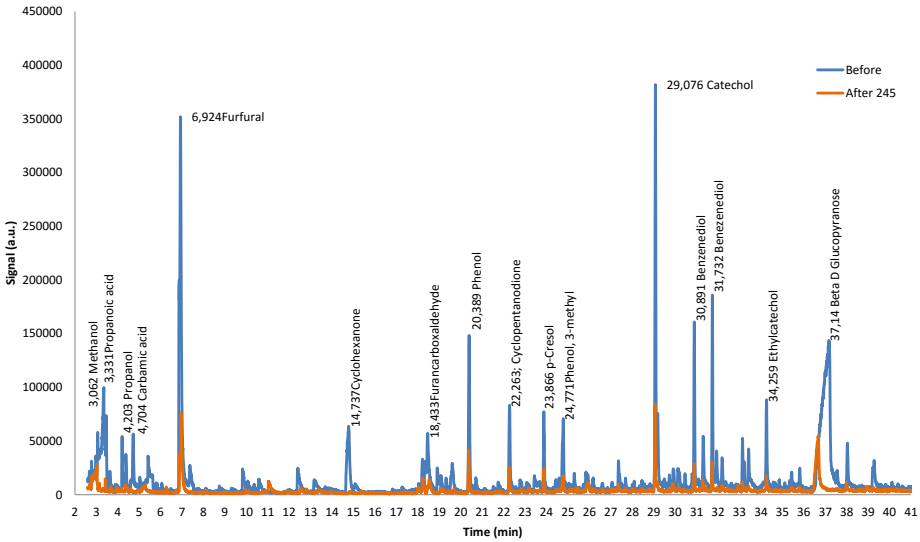

Figure 6-6.- Chromatogram before and after reaction using as a solvent THF.

Additionally, another method has been implemented to detect peaks at low retention time by adding a solvent whose retention time is higher. Since we are interested in following short length organic acids namely acetic acid and acetone, its critical for our analysis to be able to see these peaks without jeopardizing the lifetime of the detector. Using dimethylsulfoxide (DMSO) as solvent for chromatography, we were able to see acetone and acetic acid. These analysis were performed for each of the samples after reaction and the outcome is summarized in Figure 6-7.

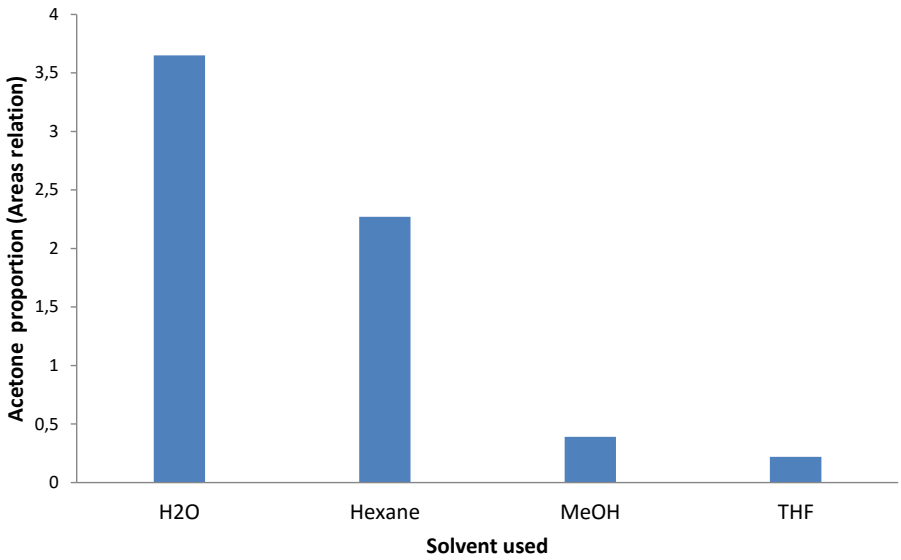

Figure 6-7.- Acetone production in terms of areas relation of 5%Ru / TiO_2 – $SiO_2$with different solvents

This result changed the appretiation of the aqueous phase results, water environments were the ones in which ketonization reaction resulted to be the most adequate. Furthermore, being waster a green solvent and at the same time the one that is present in bio-oil there was decided to be the optimum to perform short carboxylic acid conversions.

6.4. Conclusions

In this chapter, it has been analysed the different chemical compounds present in aqueous phase bio-oil. It has been studied the activity of the catalyst 5%Ru/TiO_2-SiO_2 under aqueous phase bio-oil to examine its ability to perform the reaction in real conditions. Catalytic tests indicate that this material is active for ketonization reaction even under real feeds. On the other hand, it presents the disadvantage of forming two different phases (solid and liquid) due to polymerization reactions.

The use of other solvents(e.g. n-hexane, methanol or THF), do not improve conversion of acetic acid, are not green neither present in bio-oil and trigger the interaction with other species present in bio-oil generating other products such as HMF, glycoaldehyde and no interaction respectively.

7. GENERAL CONCLUSIONS AND FUTURE CHALLENGES

Summarizing the content of this thesis in the following bullet points we will described the goals accomplished by this investigation in order to give the reader a complete vision of the results obtained and the evolution from the experiments design to decision making upon these results.

The main targets identified in this thesis are:

- From the catalyst matrix of Ru and Ni metal loading over TiO_2 and ZrO_2 supports, it has been selected 5% Ru/TiO_2 P25 as the optimum catalyst to perform ketonization in organic liquid phase.

- Optimum 1% Ru loading has been identified as the most adequate deposition amount after performing different catalytic activity measurements with different quantities of Ru, which has a direct impact on the materials cost since is by far the most expensive compound.

- Effect of TiO_2 phases (anatase, P25 and rutile) for ketonization reaction has been studied obtaining kinetics, activation energies and a complete characterization of the samples. These studies indicate a clear enhancement on dispersion of Ru in TiO_2 rutile since both present the same crystal structure (RuO_2 and TiO_2), which has been identified as interface lattice matching. Additionally, Arrhenius plots of the different catalysts reveal a lower activation energy in case of rutile vs P25 and anatase.

- Powder contact angle measurements have been conducted for different materials to test the hydrophobic or hydrophilic behavior of the catalysts and to see the influence on aqueous phase reaction. Results evidence a more hydrophobic behavior of rutile compared to P25 and anatase that had a highly hydrophilic trend. This seems to have a direct correlation with the activity of the catalyst in aqueous phase.

- 5% Ru/TiO_2P25 is quickly deactivated in liquid water. Alternatively, 5% Ru/TiO_2 rutile, present conversion in aqueous phase do to it more hydrophobic behavior.

- Reciclability of the catalyst 5% Ru/TiO_2 rutile on aqueous phase have been carried out, showing similar activity values after three runs.

- Additionally, following this hydrophobization effect core-shell materials TiO_2-SiO_2 have been studied. These solids were calcined at 800ºC to dehydroxylate the surface enhacing its hydrophobicity irreversibly. After impregnation with Ru (5 wt %), the catalysts were tested in hot liquid water showing also high conversion of model compounds (e.g. acetic acid).

- The optimum amount of SiO_2 on TiO_2 core was identified as 5%, higher values result in no interaction on the organic molecules with the titania surface. Furthermore, SiO_2 presents other advantages such as no catalytic interaction in ketonization reaction and the ability to maintain surface areas of titania even after calcination at high temperatures.

- Finally, these materials were tested under real feeds (e.g. aqueous phase bio-oil) showing similar conversion as with model compounds. However, the formation of a solid phase is not desired and further optimization studies will be needed to minimize the formation of these solids under aqueous environments.

Future challenges involve several aspects: first, the running of the reaction in hydrogen atmosphere to minimize the polymerization side reactions; second, the scale-up of the process by testing it in a continuous plug flow reactor.

Further studies could cover the effect of metal and support crystal interphase lattice matching to other reactions and catalysts to improve dispersion and activity.

Effect of calcination temperature on the hydrophobicity of materials and its influence on different reactions in aqueous phase could be another field suggested for further investigations.

8. REFERENCES

Aguado, R., Olazar, M., San José, M. J., Aguirre, G., & Bilbao, J. (2000). Pyrolysis of Sawdust in a Conical Spouted Bed Reactor. Yields and Product Composition. *Industrial & Engineering Chemistry Research*, *39*(6), 1925–1933. http://doi.org/10.1021/ie990309v

Amore Bonapasta, A., Filippone, F., Mattioli, G., & Alippi, P. (2009). Oxygen vacancies and OH species in rutile and anatase TiO2 polymorphs. *Catalysis Today*, *144*(1-2), 177–182. http://doi.org/10.1016/j.cattod.2009.01.047

Barteau, M. A. . K. K. S. (1990). Structure and Composition Requirements for Deoxygenation , Dehydration , and Ketonization Reactions of Carboxylic Acids on. *Journal of Catalysis*, *375*(125), 353.

Benvenutti, E. V, Franken, L., & Moro, C. C. (1999). FTIR Study of Hydrogen and Carbon Monoxide Adsorption on Pt / TiO 2 , Pt / ZrO 2 , and Pt / Al 2 O 3, (32), 8140–8146.

Bouzoubaa, A., Markovits, A., Calatayud, M., & Minot, C. (2005). Comparison of the reduction of metal oxide surfaces: TiO2-anatase, TiO2-rutile and SnO2-rutile. *Surface Science*, *583*(1), 107–117. http://doi.org/10.1016/j.susc.2005.03.029

CASCATBEL project. (n.d.). Retrieved May 24, 2016, from www.cascatbel.eu

Chen, H.-Y. T., Tosoni, S., & Pacchioni, G. (2015). Hydrogen Adsorption, Dissociation, and Spillover on Ru 10 Clusters Supported on Anatase TiO 2 and Tetragonal ZrO 2 (101) Surfaces. *ACS Catalysis*, *5*(9), 5486–5495. http://doi.org/10.1021/acscatal.5b01093

Gómez-Monedero, B., Bimbela, F., Arauzo, J., Faria, J., & Ruiz, M. P. (2015). Pyrolysis of Red Eucalyptus, Camelina Straw, and Wheat Straw in an Ablative Reactor. http://doi.org/10.1021/ef5026054

Hernandez-Mejia, C., Gnanakumar, E. S., Olivos-Suarez, A., Gascon, J., Greer, H. F., Zhou, W., … Raveendran Shiju, N. (2016). Ru/TiO 2 -catalysed hydrogenation of xylose: the role of the crystal structure of the support. *Catal. Sci. Technol.*, *6*(2), 577–582. http://doi.org/10.1039/C5CY01005E

Ignatchenko, A. V. (2011). Density Functional Theory Study of Carboxylic Acids Adsorption and Enolization on Monoclinic Zirconia Surfaces. *The*

Journal of Physical Chemistry C, *115*(32), 16012–16018. http://doi.org/10.1021/jp203381h

Jiang, X., & Brinker, C. J. (2010). Rigid templating of high surface-area , mesoporous , nanocrystalline rutile using a polyether block amide copolymer template w, 6123–6125. http://doi.org/10.1039/c0cc01394c

Kanta, A., Sedev, R., & Ralston, J. (2005). Thermally- and Photoinduced Changes in the Water Wettability of Low-Surface-Area Silica and Titania, (18), 2400–2407.

Liu, C., Karim, A. M., Lebarbier, V. M., Mei, D., & Wang, Y. (2013). Vapor Phase Ketonization of Acetic Acid on Ceria Based Metal Oxides. *Topics in Catalysis*, *56*(18-20), 1782–1789. http://doi.org/10.1007/s11244-013-0114-2

Lu, J., Faheem, M., Behtash, S., & Heyden, A. (2015). Theoretical investigation of the decarboxylation and decarbonylation mechanism of propanoic acid over a Ru (0 0 0 1) model surface. *Journal of Catalysis*, *324*, 14–24. http://doi.org/10.1016/j.jcat.2015.01.005

M. Ringer, V. P. P. and J. S. (2006). Large-scale pyrolysis oil production: a technology assessment and economic analysis. *Nrel/Tp-510-37779, Nrel*, (November).

Machida, M., Norimoto, K., & Watanabe, T. (1999). The effect of SiO 2 addition in super-hydrophilic property of TiO 2 photocatalyst, *4*, 2569–2574.

Mao, D., Lu, G., & Chen, Q. (2004). Influence of calcination temperature and preparation method of TiO2–ZrO2 on conversion of cyclohexanone oxime to ε-caprolactam over B2O3/TiO2–ZrO2 catalyst. *Applied Catalysis A: General*, *263*(1), 83–89. http://doi.org/10.1016/j.apcata.2003.12.028

Mohan, D., Pittman, C. U., & Steele, P. H. (2006). Pyrolysis of Wood/Biomass for Bio-oil: A Critical Review. *Energy & Fuels*, *20*(3), 848–889. http://doi.org/10.1021/ef0502397

Mukherjee, S., & Vannice, M. (2006). Solvent effects in liquid-phase reactionsI. Activity and selectivity during citral hydrogenation on Pt/SiO2 and evaluation of mass transfer effects. *Journal of Catalysis*, *243*(1), 108–130.

http://doi.org/10.1016/j.jcat.2006.06.021

Nagaoka, K., Takanabe, K., & Aika, K. (2004). Modification of Co / TiO 2 for dry reforming of methane at 2 MPa by Pt , Ru or Ni, *268*, 151–158. http://doi.org/10.1016/j.apcata.2004.03.029

Pacchioni, G. (2014). Ketonization of Carboxylic Acids in Biomass Conversion over TiO 2 and ZrO 2 Surfaces : A DFT Perspective. *ACS Catalysis*, *4*, 2874. http://doi.org/10.1021/cs500791w

Perez Ramirez, J., Mondelli, C., Schmidt, T., & Schluter, O. F. (2011). Environmental Science Sustainable chlorine recycling via catalysed HCl oxidation : from, 4786–4799. http://doi.org/10.1039/c1ee02190g

Pestman, R., Koster, R. M., Duijne, A. Van, Pieterse, J. A. Z., & Ponec, V. (1997). Reactions of Carboxylic Acids on Oxides, *272*, 265–272.

Pham, T. N., Shi, D., & Resasco, D. E. (2013a). Kinetics and Mechanism of Ketonization of Acetic Acid on Ru/TiO2 Catalyst. *Topics in Catalysis*, *57*(6-9), 706–714. http://doi.org/10.1007/s11244-013-0227-7

Pham, T. N., Shi, D., & Resasco, D. E. (2013b). Kinetics and Mechanism of Ketonization of Acetic Acid on Ru/TiO2 Catalyst. *Topics in Catalysis*, *57*(6-9), 706–714. http://doi.org/10.1007/s11244-013-0227-7

Pham, T. N., Shi, D., Sooknoi, T., & Resasco, D. E. (2012). Aqueous-phase ketonization of acetic acid over Ru/TiO2/carbon catalysts. *Journal of Catalysis*, *295*, 169–178. http://doi.org/10.1016/j.jcat.2012.08.012

Pham, T. N., Sooknoi, T., Crossley, S. P., & Resasco, D. E. (2013). Ketonization of Carboxylic Acids: Mechanisms, Catalysts, and Implications for Biomass Conversion. *ACS Catalysis*, *3*(11), 2456–2473. http://doi.org/10.1021/cs400501h

Puértolas, B., Keller, T. C., Mitchell, S., & Pérez-Ramírez, J. (2016). Deoxygenation of bio-oil over solid base catalysts: From model to realistic feeds. *Applied Catalysis B: Environmental*, *184*(MAY), 77–86. http://doi.org/10.1016/j.apcatb.2015.11.017

Pulido, A., Oliver-Tomas, B., Renz, M., Boronat, M., & Corma, A. (2013). Ketonic decarboxylation reaction mechanism: a combined experimental and DFT study. *ChemSusChem*, *6*(1), 141–51.

http://doi.org/10.1002/cssc.201200419

Schwartz, T. J., Neill, B. J. O., Shanks, B. H., & Dumesic, J. A. (2014). Bridging the Chemical and Biological Catalysis Gap: Challenges and Outlooks for Producing Sustainable Chemicals.

Serrano-Ruiz, J. C., & Dumesic, J. a. (2011). Catalytic routes for the conversion of biomass into liquid hydrocarbon transportation fuels. *Energy & Environmental Science*, *4*(1), 83. http://doi.org/10.1039/c0ee00436g

Teipel, U., & Mikonsaari, I. (2004). Determining contact angles of powders by liquid penetration. *Particle and Particle Systems Characterization*, *21*(4), 255–260. http://doi.org/10.1002/ppsc.200400931

Tessarolo, N. S., Silva, R. V. S., Vanini, G., Casilli, A., Ximenes, V. L., Mendes, F. L., … Azevedo, D. A. (2015). Characterization of thermal and catalytic pyrolysis bio-oils by high-resolution techniques: 1H NMR, GC×GC-TOFMS and FT-ICR MS. *Journal of Analytical and Applied Pyrolysis*, 1–11. http://doi.org/10.1016/j.jaap.2015.11.007

Ti, H., Tosoni, S., & Pacchioni, G. (2015). Adsorption of Ruthenium Atoms and Clusters on Anatase TiO 2 and Tetragonal ZrO 2 (101) Surfaces : A Comparative DFT Study, *2*(101).

Tosoni, S., Civalleri, B., & Ugliengo, P. (2010). Hydrophobic Behavior of Dehydroxylated Silica Surfaces : A B3LYP Periodic Study, 19984–19992.

Wu, S. (2015). Estimation and comparison of bio-oil components from different pyrolysis conditions, *3*(June), 1–11. http://doi.org/10.3389/fenrg.2015.00028

Xu, M., Iglesia, E., Apestegu, C. R., Cosimo, D. I., & Al, E. T. (1998). Structure and Surface and Catalytic Properties of Mg-Al Basic Oxides, *510*, 499–510.

Yang, C., Yu, Y., Linden, B. Van Der, & Wu, J. C. S. (2010). Artificial Photosynthesis over Crystalline TiO 2 -Based Catalysts : Fact or Fiction ?, *74*(13), 8398–8406.

Zhang, L., Chen, K., Chen, B., & Resasco, D. E. (2015). Factors that Determine Zeolite Stability in Hot Liquid Water. http://doi.org/10.1021/jacs.5b07398

Zhu, X., Lobban, L. L., Mallinson, R. G., & Resasco, D. E. (2010). Tailoring the mesopore structure of HZSM-5 to control product distribution in the conversion of propanal. *Journal of Catalysis*, *271*(1), 88–98. http://doi.org/10.1016/j.jcat.2010.02.004

9. APPENDIX A

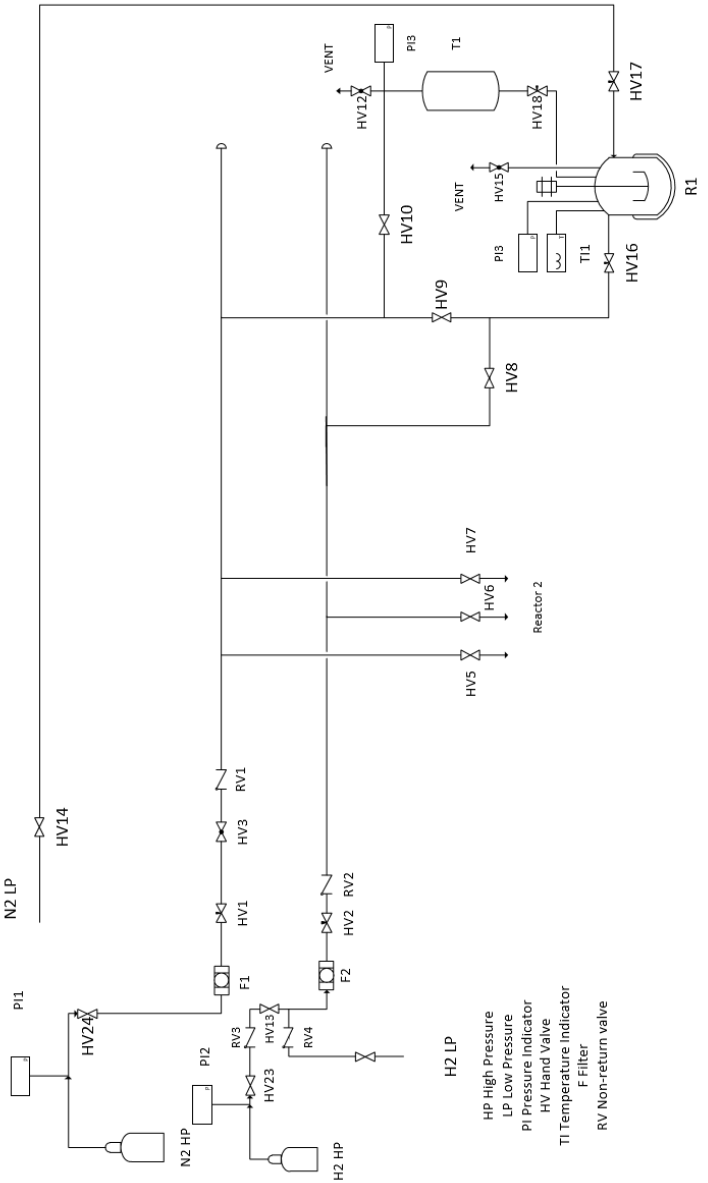
N2 LP
HV14
PI1
HV24
N2 HP
PI2
RV3
HV13
RV4
HV23
H2 HP
H2 LP
F1
F2
HV1
HV2
RV1
RV2
HV3
HV7
HV6
HV5
Reactor 2
HV8
HV9
HV10
VENT
HV12
PI3
T1
HV18
HV17
R1
VENT
HV15
PI3
TI1
HV16
HP High Pressure
LP Low Pressure
PI Pressure Indicator
HV Hand Valve
TI Temperature Indicator
F Filter
RV Non-return valve

10. APPENDIX B

10.1. Calculation of powder contact angle of TiO_2 P25

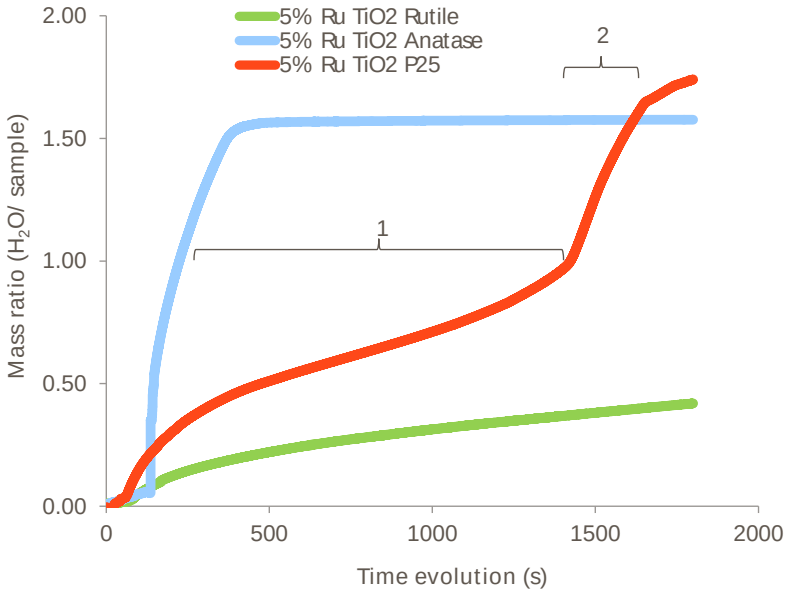

Figure B-1. Mass ratio of H2O:sample as function of time during powder contact angle measurement of 5 wt. % Ru supported on TiO2 rutile (green), P25 (red), and anatase (blue).

Based on the paper of Teipel et al. it was indicated: "The linear region of the obtained time dependent curves represents the wetting process and its kinetics. Therefore, we further determined:

$$\alpha = \frac{m_l}{A \cdot \sqrt{t}} = \sqrt{\frac{\rho_t^2 \cdot \kappa \cdot \gamma_{lv} \cdot \cos\theta}{2 \cdot \eta_l}} = \sqrt{\frac{\rho_t^2 \cdot \gamma_{lv}}{2 \cdot \eta_l}} \cdot \sqrt{\kappa \cdot \cos\theta}$$

$$= \alpha_1 \cdot \alpha_2 \quad (1)$$

Therefore we calculate α for each of the section of the curve above described:

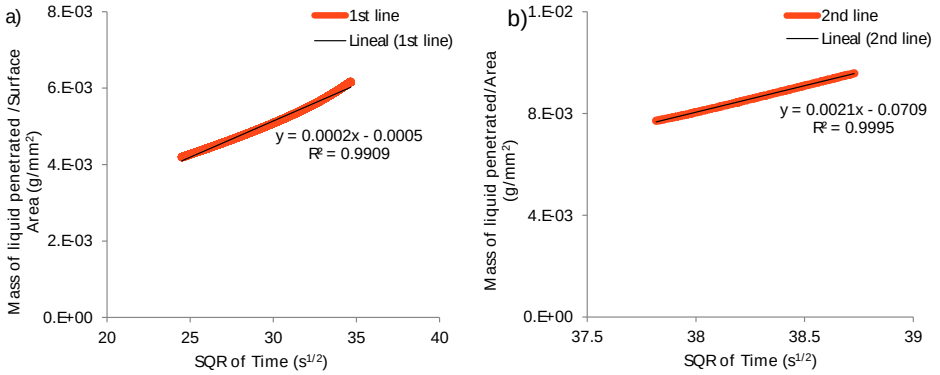

Figure B-2. Mass ratio of H_2O: sample as function of square root of (SQR) time during powder contact angle measurement of 5 wt. % Ru supported on TiO2 P25 of the section 1 (a) and section 2 (b) of the powder contact angle measurement.

From Figure B-2-a we obtained

$$\alpha_{\text{Section 1}} = 0.0002$$

And from Figure B-2-b

$$\alpha_{\text{Section 2}} = 0.0021$$

Taking two different regions, and dividing equation (1), and due to the fact that

we have same factors, fluid, surface tension we can simplify it to:

$$\frac{\alpha_{\text{Section 1}}}{\alpha_{\text{Section 2}}} = \frac{\sqrt{k \cos \theta_1}}{\sqrt{k \cos \theta_2}} \quad (2)$$

Subsequently,

$$\left(\frac{\alpha_{\text{Section 1}}}{\alpha_{\text{Section 2}}}\right)^2 = \frac{\cos \theta_1}{\cos \theta_2} \quad (3)$$

Knowing that poder contact angle in stretch 1 is 89.47°, it can be determined θ_2 by using expression (3);

$\theta_2 = 43°$(powder contact angle of section 2)

Assuming that the contact angle of the material can be described as linear combination of the two surfaces wettability then one can calculate the contact angle as follows:

$$\theta_{P25} = X_{\text{anatase}} * \theta_2 + X_{\text{rutile}} * \theta_1$$

Utilizing the ratio of anatase: rutile of 80:20 we get the following contact angle:

$$\theta_{P25} = 52.29°$$